Environmental Science and Pollution Research (2022) 29:15681–15702
https://doi.org/10.1007/s11356-021-16789-9

RESEARCH ARTICLE

# Spatio-temporal evolution of post-seismic landslides and debris flows: 2017 $M_s$ 7.0 Jiuzhaigou earthquake

Xianmin Wang[1] · Hang Mao[1]

Received: 3 May 2021 / Accepted: 23 September 2021 / Published online: 11 October 2021


## Abstract

Spatio-temporal evolution of post-seismic landslides and debris flows provides a new perspective to understand post-earthquake evolution of geological environments and landscapes, and to instruct cascaded catastrophic hazard mitigation and post-disaster reconstruction. However, limited earthquake events have been investigated for post-earthquake geohazard evolution. This work reports the geohazard evolution after the 2017 $M_s$ 7.0 Jiuzhaigou earthquake considering the effects of the earthquake, geology, terrain, meteorology, hydrology, and human engineering activity. Some new viewpoints are suggested. (1) Landslide and debris flow activity intensified in the first year following the earthquake under the effects of the antecedent earthquake, precipitation, fault tectonics, human engineering activity, and fluvial networks. (2) Landslide and debris flow activity declined rapidly in the second year as a result of dramatically reduced sediments, declined rainfall, and self-healed slopes. (3) The significant decay of landslide and debris flow activity and the prominent reduction of loose deposits indicate that the geological environment was gradually restoring. (4) Although the hazard effect mitigation and geological environment restoration were ongoing (in the absence of rainstorm events) to attain a new balance, the geoenvironment has not returned to the pre-earthquake level because of widespread unrecovered geohazards and the remaining loose deposits on hillslopes or in channels. (5) The geological environment after the Jiuzhaigou earthquake may re-equilibrate and return to the pre-earthquake level more quickly than after the Kashmir, Chi-Chi, Gorkha, Wenchuan, and Murchison earthquakes. This work provides new knowledge pertaining to geohazard evolution after a strong earthquake and to profound impacts of a catastrophic earthquake on geological environment and landscape.

**Keywords** Landslide evolution · Debris flow evolution · Earthquake · Jiuzhaigou · Geological environment

## Introduction

Post-seismic landslides and debris flows (PSLDs) are characterized by large quantities, large scales, broad and concentrated distribution, great damage, and cascaded high risks (Xu 2018), and have received close attention from scientists (Keefer 1984; Zhang et al. 2014; Fan et al. 2019; Papathanassiou et al. 2021; Comert 2021; Porta et al. 2021; Koukouvelas et al. 2020; Litoseliti et al. 2020). PSLDs generate widespread mass wasting (Avouac 2007) and play a significant erosional and depositional role in relief reduction (Hovius et al. 2011) during the years to decades following earthquakes (Nakamura et al. 2000; Lin et al. 2006; Lin et al. 2008; Li et al. 2018). Thus, they exert a far-reaching influence on the long-term evolution of geological environment and landscape (Malamud et al. 2004; Fan et al. 2018; Broeckx et al. 2020). Moreover, the sudden and collective outbursts of PSLDs are conspicuously enhanced because of the relaxation and destruction of mountain rock mass caused by earthquakes (Huang 2011). These landslide and debris flow activities and impacts may extend several years (for example, the 2005 $M_w$ 7.6 Kashmir earthquake) (Saba et al. 2010) or even over 50 years (like the 1929 $M_w$ 7.7 Murchison earthquake) (Pearce and Watson 1986) before the impacted regions revert to stability. In addition, the

Responsible Editor: Philippe Garrigues

✉ Xianmin Wang
xianminwang@163.com

[1] Hubei Subsurface Multi-scale Imaging Key Laboratory, Institute of Geophysics and Geomatics, State Key Laboratory of Biogeology and Environmental Geology, China University of Geosciences, Wuhan 430074, China

aggravation of landslide and debris flow activity after earthquakes poses long-term dangers to human lives and critical infrastructures in large-scale earthquake-struck areas. This has always been an enormous challenge for long-term prevention and cure of geological disasters. Therefore, it is crucial to reveal the spatio-temporal evolution of PSLDs to better understand the geological environment and landscape development after earthquakes, to effectively mitigate the cascaded high risk of PSLDs, and to rationally instruct post-disaster reconstruction (Huang 2011). However, thus far, limited earthquake events have been investigated in terms of landslide and debris flow evolution after these catastrophic earthquakes, such as the 1929 $M_w$ 7.7 Murchison earthquake, 1993 $M_w$ 6.9 Finisterre earthquake, 1999 $M_w$ 7.6 Chi-Chi earthquake, 2004 $M_w$ 6.6 Niigata earthquake, 2005 $M_w$ 7.6 Kashmir earthquake, 2008 $M_w$ 7.9 Wenchuan earthquake, 2008 $M_w$ 6.8 Iwate earthquake, 2008 $M_w$ 6.4 Movri Mountain earthquake, and 2015 $M_w$ 7.8 Gorkha earthquake (e.g., Pearce and Watson 1986; Hovius et al. 2011; Khan et al. 2013; Marc et al. 2015; Chang et al. 2015; Li et al. 2018; Yang et al. 2018a; Shafique 2020; Tian et al. 2020; Litoseliti et al. 2020; Basharat et al. 2021).

The evolution and restoration period of PSLDs varies distinctly in different earthquake-affected regions and are highly dependent on earthquake magnitude, geology, topography, geomorphology, material composition, and climate (Huang 2011; Zhang and Zhang 2017; Hu et al., 2019; Tian et al. 2020). In some earthquake-struck regions, the PSLDs were remarkably strengthened and highly activated for decades (Huang 2011). For example, the landslides caused by the 1923 $M_w$ 7.9 Kanto earthquake were highly active for approximately 15 years and returned to stability after 40–50 years (Nakamura et al. 2000). The landslides induced by the 1929 $M_w$ 7.7 Murchison earthquake supplied ~400,000-$m^3/km^2$ stream channel sediments and at least 50–75% of the granitic debris was still trapped in the fourth-order catchment 50 years after the earthquake (Pearce and Watson 1986). After 7–8 years of evolution after the 2008 $M_w$ 7.9 Wenchuan earthquake, the debris flows and landslides still remained active at higher levels than the pre-earthquake levels (Tang et al. 2016; Zhang and Zhang 2017; Fan et al. 2018a, 2018b; Liu et al. 2018a, 2018b) and would continue to remain active for a long time due to massive loose deposits and seasonal rainfall (Cui et al. 2011; Zhang et al. 2016; Zhang and Zhang 2017; Li et al. 2018; Yang et al. 2018a). However, in some earthquake-impacted areas, the activity of PSLDs rapidly decayed to pre-earthquake levels within years. For example, the enhanced landslide activity following the 2005 $M_w$ 7.6 Kashmir earthquake remained at a high level for no more than 2 years and progressively approached a new stable condition within 2–5 years after the earthquake, with most slopes returning to equilibrium (Saba et al. 2010; Khattak et al. 2010; Khan et al. 2013; Shafique 2020). The density of rainfall-triggered landslides obviously increased 1–2 years after the 1999 $M_w$ 7.6 Chi-Chi earthquake (Lin et al. 2006), and the mass wasting and fluvial sediment evacuation ever reached more than 5 times the background rate and gradually recovered to pre-earthquake levels after approximately 6 years (Hovius et al. 2011). Landslide rates after three shallow thrust earthquakes, i.e., the 1993 $M_w$ 6.9 Finisterre earthquake, 2004 $M_w$ 6.6 Niigata earthquake, and 2008 $M_w$ 6.8 Iwate earthquake, peaked and then decreased to background values respectively within 1.5–2.7 years, 0.5–0.9 years, and 1.0–2.4 years, with the decay time scale possibly associated with the earthquake magnitude and decreased transient ground strength (Marc et al. 2015). Therefore, the evolutionary characteristics and period of PSLDs vary significantly in diverse earthquake-attacked regions, even under approximate seismic magnitudes.

The 2017 $M_s$ 7.0 Jiuzhaigou earthquake occurred in the middle of the famous north-south seismic belt in China where earthquakes have intensively happened (Li et al. 2017). The earthquake occurred at the intersection of the Tazang, Huya, and Minjiang faults on the eastern margin of the Bayan Har block in the Tibet Plateau (Xu et al. 2017). Historically, 26 earthquakes above $M_s$ 5.0 and 9 earthquakes above $M_s$ 7.0 struck the area within 200 km from the Jiuzhaigou epicenter (The Earthquake Disaster Prevention Department of China Earthquake Administration 1995, 1999; Lei et al. 2018; Fang et al. 2018). The earthquake-attacked areas are characterized by extremely complicated geological and topographic conditions, such as developed folds and fractures, intensive neotectonic movements, widespread carbonates, large-scale karst tufa deposits, uplifted crust, and large terrain transformation from the Tibet Plateau to the Sichuan Basin (Lei et al. 2018). Therefore, research on the evolution of landslides and debris flows after the Jiuzhaigou earthquake has significant geological implications in revealing the PSLD development rule in an ultracomplex geological and topographic context. Moreover, the Jiuzhaigou Valley within the earthquake-influenced region, a world-famous scenic spot, has been selected as a UNESCO World Natural Heritage Site and a World Biosphere Reserve (UNESCO 1992; Fan et al. 2018). In 2016, the annual tourist number surpassed 5 million, accompanied by tourism revenue of CNY 805 million (SBNESD, 2016). In this world-popular tourist attraction, some scenic spots reopened on September 27, 2019. Thus, an insight into the PSLD evolution has important social and economic merits in safeguarding tourists, villages, roads, and human infrastructure with frequent human activities. Therefore, because of the unique and critical significance of geology, society, and economy, the evolution of landslides and debris flows after the Jiuzhaigou earthquake is studied to improve the understanding of PSLD development considering the effects of earthquake, geology, terrain, hydrology, meteorology, and human engineering activity.

Research on Jiuzhaigou earthquake-triggered hazards has covered four main aspects. (1) The spatial distribution patterns of coseismic landslides and debris flows were investigated mainly via remote sensing technique (e.g., Dai et al. 2017; Xu et al., 2018; Fan et al. 2018; Wu et al., 2018; Cheng et al. 2018; Tian et al. 2019; Dong et al. 2019; Chang et al. 2021). Some studies suggested that the spatial pattern of Jiuzhaigou coseismic landslides was substantially affected by topographic amplification of seismic waves, including back slope and thin ridge effects (Zhao et al. 2018; Wu et al., 2018; Wang et al. 2018; Shen et al. 2019; Liang et al. 2019). (2) The susceptibility of coseismic landslides was evaluated using remote sensing, seismic, geologic, topographic, and coseismic landslide data (Dai et al. 2017; Fan et al. 2018; Cao et al. 2019; Yi et al. 2019; Cao et al. 2020; Chen et al. 2020). Moreover, risk identification and evaluation were conducted to investigate the impact of post-earthquake landslides or rockfalls on roads (Yue et al. 2018; Li et al. 2019). (3) The variation trend and the potential danger of PSLDs were evaluated according to the damage from the coseismic geological hazards (Chen et al. 2018; Hu et al. 2019a). Chen et al. (2018) delineated the coseismic geohazards of 13 landslides, 70 collapses, and 25 potential debris flow gullies in the Jiuzhaigou Valley. Based on the rain intensity cycle in the Jiuzhaigou Valley and the geohazard variation tendencies triggered by the Kanto, Chi-Chi, and Wenchuan earthquakes, it was predicted that Jiuzhaigou PSLD activity may last over 10 years and would progressively attenuate back to pre-earthquake levels in 5 to 10 years (Chen et al., 2018). Hu et al. (2019a) highlighted 83 coseismic landslides in the Jiuzhaigou Valley and suggested that the PSLD activity recovery period in Jiuzhaigou would be shorter than that in Chi-Chi and Wenchuan because of the small hazard magnitude and better geological condition. (4) The serious destruction caused by coseismic geohazards to natural landscapes was quantitatively evaluated in the Jiuzhaigou Valley (Hu et al. 2019b).

A considerable amount of new knowledge has been acquired on the coseismic landslides and debris flows in the Jiuzhaigou area; however, the spatio-temporal evolution of PSLDs has not been specifically revealed. This work employs multisource data (seismic, geologic, topographic, meteorological, and remote sensing data) and field investigation to reveal the spatio-temporal development of PSLDs from August 2017 to August 2019 under the effects of earthquake, geology, terrain, rainfall, drainage system, and human engineering activity. New insights into the following questions are suggested: (1) How did the landslides and debris flows evolve after the earthquake? (2) Which influencing factors controlled or induced these evolutions? (3) What are the spatio-temporal evolution rule and trend of the PSLDs? Answers to these questions can improve our limited understanding of the geohazard evolution after a violent earthquake and supplement new knowledge on the profound impact of catastrophic earthquakes on landscape and geological environment.

## Study area

On August 8th, 2017, a strong $M_s$ 7.0 earthquake attacked Jiuzhaigou County in China with an epicenter at 33.20° N, 103.82° E and a focal depth of 20 km (CENC 2017). This earthquake caused a direct economic loss of up to CNY 22.45 billion and resulted in 25 deaths, 525 casualties, 6 missing people, 176,492 vulnerable people, and 73,671 damaged buildings by 8:00 pm August 13, 2017 (Fan et al. 2018; Xu et al., 2018; Hu et al., 2019). The intensive distribution region of the earthquake-induced landslides and debris flows is selected as the study area (Figure 1) to reveal the spatio-temporal evolution feature and rule of the PSLDs.

The study area, covering a region of 938.9 $km^2$, is situated at the northern edge of the Minshan Block bordering the Longmenshan Range, Huya, Tazang, and Minjiang fractures in the south, east, north, and west, respectively (Zhao et al. 2018). A critical seismic belt, with multiple strong earthquakes ($M_s \geq 7.0$), spreads along the block boundaries making it one of the most active tectonic units in China (Sun et al. 2018; Zhao et al. 2018). Thus, the active fault structures are extremely intricate under the strong compression of shear stress in the study area (Xu et al. 2017; Li et al. 2017). The blind seismogenic fault, striking ~152° and dipping ~70° across the study area, is dominated by a NW-SE-oriented left-lateral strike-slip movement (CENC 2017; Li et al. 2017; Yi et al., 2017) and is attributed to an eastern branch fracture in the East Kunlun fault zone (Yi et al., 2017). The study area stretches across the regions of seismic intensities of IX, VIII, and VII, with the main shock peak ground acceleration (PGA) varying from 0.12 to 0.26 g. The neotectonic movement is intense and forms NE-oriented and NS-oriented tectonic systems composed of anticlinoria and synclinoria (Cheng et al. 2018). Limestone prevails regionally, accompanied by exposed Devonian, Carboniferous, Permian, Triassic, Tertiary, and Quaternary system strata (Liu G. et al., 2018).

The study area, abundant in deep-incised ravines and gullies, features alpine canyon landforms that were shaped and eroded by tectonic, glacial, and hydrological activities (Fan et al. 2018). The terrain elevation gradually varies downward from southwest to northeast with the highest elevation of 4570 m and an average slope angle of 31°. The high mountains, steep terrain, abundant precipitous surfaces, and developed river systems favor landslide and debris flow development (Liu et al., 2018). A mass of loose deposits and sediments, generated from the strong earthquake and secondary hazards, supply rich source materials for the post-seismic new landslides and debris flows. The annual rainfall (2017–2019) was relatively low in the study area (~677–~730 mm) mainly concentrated from May to October. Moreover, road construction and tourism development may play important anthropic roles in landslide and debris flow occurrences in the study area (Wang et al. 2018; Cao et al. 2019).

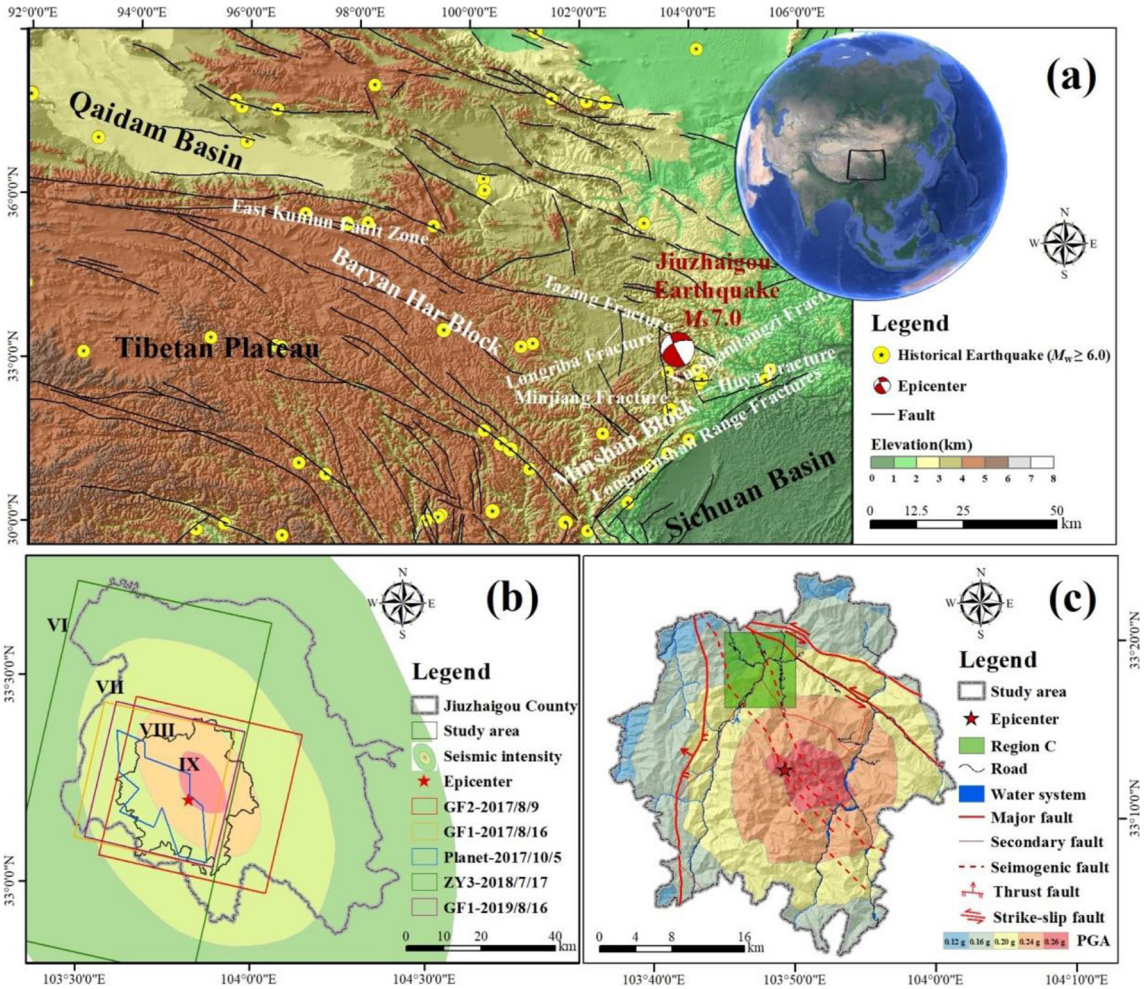


**Figure 1** Seismotectonic setting of Jiuzhaigou County and the study area. **a** Jiuzhaigou earthquake and the complicated seismotectonic setting. **b** Study area in Jiuzhaigou County. The seismic intensity and the acquisition times and scopes of the high-resolution remote sensing images are indicated. **c** Seismotectonic setting of the study area and the distributions of roads and river systems. The inferred seismogenic fault is from Li et al. (2017). The historical earthquake data are from the United States Geological Survey, and the fault data are from National Geological Archive. The Earth picture is from Google Earth. The administrative boundary of Jiuzhaigou County is from Geographical Information Monitoring Cloud Platform.

## Data and methods

### Multisource data

Five sets of multisource data are employed to investigate geohazards and mass wasting and to establish various influencing factors closely related to landslide and debris flow evolution (Table 1). (1) Multi-temporal high-resolution remote sensing images (Gaofen-1, Gaofen-2, Planet, Ziyuan-3, and Google images) are used to delineate the geohazards, hillslope deposits, and channel deposits generated during and after the earthquake. Thus, geohazard evolution and mass wasting can be revealed. Additionally, multi-temporal Sentinel-2 images, combined with the other high-resolution images, are adopted to establish the critical influencing factors of human engineering activity, environment, and hydrology in 2018 and 2019, including land use, distance to road, normalized difference vegetation index (NDVI), and distance to the river. (2) Seismic data are utilized to construct the seismic factors of PGA, seismic intensity, distance to epicenter, and distance to seismogenic fault. (3) Geological maps are used to build the geological and tectonic factors of lithology, fault density, and distance to the fault. (4) Digital elevation model (DEM) data are adopted to produce the topographic factors of elevation, slope angle, and aspect. (5) Meteorological data are employed to establish the precipitation factors of cumulative rainfall, maximum cumulative rainfall, minimum cumulative rainfall, and maximum cumulative rainfall in continuous precipitation events in 2017, 2018, and 2019. Therefore, by synthesis of geohazard development, mass wasting, and various influencing factors, the spatio-temporal evolution characteristics, rule, and trend of PSLDs can be revealed.

**Table 1** Multisource data for coseismic and post-seismic landslides and debris flows

| Data type | Data | Date | Resolution | Source |
|---|---|---|---|---|
| Image | Gaofen-1 | 16 August 2017; 16 August 2019 | 2 m | China Center for Resources Satellite Data and Application |
| | Gaofen-2 | 09 August 2017 | 1 m | |
| | Ziyuan-3 | 17 July 2018 | 2 m | |
| | Planet | 05 October 2017 | 4 m | Planet Labs |
| | Google Image | 01 October 2015; 16 October 2015; 21 October 2015; 7 December 2015; 13 August 2017; 14 August 2017; 14 December 2018; 27 September 2019 | 0.32–0.54 m | Google Earth |
| | Sentinel-2 | 29 July 2017; 7 September 2017; 23 August 2018; 27 September 2019 | 10 m | European Space Agency |
| Terrain | Digital elevation model (DEM) | 13 February 2011 | 12.5 m | National Aeronautics and Space Administration |
| Geology | Geological map | Pre-earthquake | 1:200,000<br>1:50,000 | China Geological Survey |
| Meteorology | Tropical Rainfall Measuring Mission (TRMM) Satellite | August 2016–July 2019 | 0.05°× 0.05° | National Aeronautics and Space Administration |
| Earthquake | Peak ground acceleration (PGA) | 08 August 2017 | - | United States Geological Survey |
| | Seismic intensity | 08 August 2017 | | China Earthquake Administration |
| | Epicenter | 08 August 2017 | | China Earthquake Networks Center |
| | Seismogenic fault | 08 August 2017 | | Li et al. 2017 |

## Methods

### Establishment of geo-environmental factors and triggering factors

Two types of influential factors closely relevant to geohazard evolution are established: geo-environmental factors controlling hazard evolution and triggering factors inducing disaster development (Table 2). The geo-environmental factors comprise seismic, geological, tectonic, topographic, and environmental factors, in which environmental factors are embodied in vegetation growth and river system and comprise the indices of NDVI and distance to river. The triggering factors include precipitation and human engineering activity factors, in which human engineering activity factors are reflected by land utilization and road construction and contain the indices of land use and distance to the road.

### Classification of geohazard evolution

Post-earthquake vegetation growth and recovery illuminate the decay and restoration of PSLDs and highlight the stability tendency of the landscape and geological environment (Yang et al. 2018a; Li et al. 2018; Fan et al. 2019; Yunus et al. 2020). Vegetation regeneration, as an indicator of geohazard decay, has been applied in geohazard restoration investigations after the Wenchuan (Lu et al. 2012; Li et al. 2018; Domènech et al. 2019), Chi-Chi (Shou et al., 2011), and Kashmir earthquakes (Shafique et al., 2020; Basharat et al. 2021). The landslide (rockfall) evolution in the study area is divided into five classes (with reference to Li et al. 2018): (1) recovered or basically recovered landslides, (2) recovering landslides, (3) active landslides, (4) unchanged landslides, and (5) new landslides. Recovered or basically recovered landslides are those that are completely covered by thick vegetation. Recovering landslides mean those that are partly covered by vegetation without area expansion. Active landslides are those with increasing areas. Unchanged landslides signify the ones maintaining the same area with no vegetation growth. New landslides mean newly occurring landslides.

The debris flow evolution in the study area falls into four categories (with reference to Li et al. 2018): (1) active debris flows, (2) new debris flows, (3) recovered debris flows, and (4) unvaried debris flows. Active debris flows occur multiple times or undergo increased areas and abundant/increased source materials. New debris flows are the newly emerging ones generated from landslide deposits and/or from channel-bed failure, which arises from bed incision, lateral bank failure, bed erosion, and rainfall (Zhang and Zhang 2017). Recovered debris flows mean debris flow gullies where the vegetation is growing well. Unvaried debris flows are debris flow gullies unaccompanied by enlarged areas and vegetation growth.

The volume of coseismic geohazards is calculated according to Equation (1) (Guzzetti et al., 2009), and this equation was established according to 677 landslides from a global landslide database (Guzzetti et al., 2009). The relationship between geohazard area and volume is generally independent of the physiographic setting (Guzzetti et al., 2009).

$$V = 0.074 \times A^{1.450} \quad (1)$$

where $V$ and $A$ are the volume and area of a geohazard, respectively.

## Results

### Landslide and debris flow investigation

The geohazards in the study area mainly consist of landslides (rockfalls) and debris flows, which are interpreted from multitemporal high-resolution remote sensing images from October 2015 to September 2019 and validated by field investigation. The distributions and statistics of coseismic geohazards and PSLDs in both Jiuzhaigou County and the study area are shown in Table 3 and Figs. 2 and 3, respectively. As shown, the earthquake-triggered geohazards in Jiuzhaigou County were intensively distributed in the study area. The field survey route is shown in Figure S1 in the supplementary file, and 257 geohazards were validated, including 214 landslides and 43 debris flows. Moreover, rainfall had an important influence on coseismic geohazards and PSLDs, and the pre-earthquake and post-earthquake rainfall statistics in the study area are shown in Figure 4.

The Jiuzhaigou earthquake triggered 5563 coseismic geohazards in the study area covering 10.83 $km^2$ and generated two hazard-dense regions: region A to the northwest of the epicenter covering 68.24 $km^2$ with an epicenter distance of 8.45 km and region B to the southeast of the epicenter covering 48.57 $km^2$ with an epicenter distance of 5.07 km (Figure 2a). These coseismic geohazards consisted of 5431 landslides with a total volume of $34.76\times10^6 m^3$ and 132 debris flows with a gross volume of $7.85\times10^6 m^3$. These coseismic geohazards were dominated by small sizes, falling in a region of 938.9 $km^2$ and generally spread along the seismogenic fault. Interestingly, 90.87% of the geohazards were located in the area with relatively abundant anterior rainfall, that is, with the accumulated rainfall larger than 590 mm from August 2016 to July 2017 (Figure 2a). The pre-earthquake rainfall had infiltrated into the rock and soil, sharply increasing pore pressures, decreasing shear strength, and facilitating the slope materials to slide and run out under the strong earthquake (Sassa et al. 2007; Faris and Wang 2014; Fan et al. 2019). Therefore, except for the triggering factor of earthquake, antecedent

**Table 2** Geo-environmental and inducing factors associated with landslide and debris flow evolution in the study area

| Factor type | | No. | Factor | Level | Data source |
|---|---|---|---|---|---|
| Geo-environmental factor | Seismic | 1 | Peak ground acceleration (PGA) (g) | (1) 0.26; (2) 0.24; (3) 0.2; (4) 0.16; (5) 0.12 | United States Geological Survey |
| | | 2 | Distance to seismogenic fault (km) | (1) <1; (2) 1~2; (3) 2~3; (4) 3~4; (5) 4~5; (6) 5~6; (7) ≥6 | Li et al. 2017 |
| | | 3 | Distance to epicenter (km) | (1) <5; (2)5–10;(3)10–15;(4) ≥15 | China Earthquake Networks Center |
| | | 4 | Seismic intensity (degree) | (1) VII; (2) VIII; (3) IX | China Earthquake Administration |
| | Geological | 5 | Lithology | (1) C; (2) $C_2$; (3) $D_{1\text{-}2}$; (4) $D_2$; (5) P; (6) $P_2$-$T_1$; (7) Q; (8) $Q_h$; (9) $Q_p$; (10) $T_1$; (11) $T_2$; (12) $T_3$; (14) $T_\gamma$ | Geological map; Li et al. 2017 |
| | Tectonic | 6 | Distance to fault (km) | (1) <0.5; (2) 0.5~1; (3) 1~1.5; (4) 1.5~2; (5) 2~3; (6) 3~4; (7) 4~5; (8) 5~6; (9) ≥6 | |
| | | 7 | Fault density ($\times 10^{-2}$ km/km$^2$) | (1) 0–5.4; (2) 5.4–15.4; (3) 15.4–25.8; (4) 25.8–36.0; (5) 36.0–46.6; (6) 46.6–60.4 | |
| | Topographic | 8 | Elevation (m) | (1) <2250; (2) 2250~2500; (3) 2500~2750; (4) 2750~3000; (5) 3000~3250; (6) 3250~3500; (7) 3500~3750;(8) 3750~4000; (9) 4000~4250; (10) ≥ 4250 | Digital elevation model(DEM) |
| | | 9 | Slope angle (degree) | (1) <10; (2) 10~20; (3) 20~26; (4) 26~32; (5) 32~38; (6) 38~45; (7) 45~55; (8) 55~90 | |
| | | 10 | Slope aspect | (1) Flat; (2) N; (3) NE; (4) E; (5) SE; (6) S; (7) SW; (8) W; (9) NW | |
| | Environmental | 11 | Distance to river (m) | (1) <200; (2) 200~400; (3) 400~600; (4) 600~800; (5) 800~1000; (6) 1000~2000; (7) 2000~3000; (8) 3000~4000; (9) ≥4000 | Gaofen-1; Ziyuan-3; Gaofen-2; Planet; Google images; Setinel-2 |
| | | 12 | Normalized difference vegetation Index (NDVI) | (1) <0.2; (2) 0.2~0.4; (3) 0.4~0.6; (4) 0.6~0.8; (5) 0.8~1.0 | Sentinel-2 |
| Triggering factor | Human activity | 13 | Land use | (1) Woodland; (2) grassland; (3) bare land; (4) wetland; (5) water; (6) construction land; (7) arable land | Sentinel-2 |
| | | 14 | Distance to road (m) | (1) <200; (2) 200~400; (3) 400~600; (4) 600~800; (5) 800~1000; (6) 1000~2000; (7) 2000~3000; (8) 3000~4000; (9) ≥4000 | Gaofen-1; Ziyuan-3; Gaofen-2; Planet; Google images; Setinel-2 |
| | Meteorological | 15 | Cumulative precipitation (mm) | August 2016 ~ July 2017: (1) <560; (2) 560~570; (3) 570~580; (4) 580~590; (5) 590~600; (6) 600~610; (7) ≥610<br>August 2017 ~ July 2018: (1) < 810; (2) 810~820; (3) 820~830; (4) 830~840; (5) 840~850; (6) 850~860; (7) 860~870; (8) 870~880; (9) 880~890; (10) ≥890<br>August 2018 ~ July 2019: (1) <580; (2) 580~590; (3) 590~600; (4) 600~610; (5) 610~620; (6) 620~630; (7) ≥630 | Tropical Rainfall Measuring Mission (TRMM) Satellite |

The lithology symbols: $P_2$-$T_1$, Middle Permian-Lower Triassic series; $T_1$, Lower Triassic series; $T_3$, Upper Triassic series; $T_2$, Middle Triassic series; $T_\gamma$, Triassic granite; $C$, undifferentiated Carboniferous system; $C_2$, Middle Carboniferous series; $D_{1\text{-}2}$, Lower-Middle Devonian series; $D_2$, Middle Devonian series; $P$, undifferentiated Permian system; $P_2$, Middle Permian series; $Q$, undifferentiated Quaternary system; $Q_h$, undifferentiated Holocene series; $Q_p$, undifferentiated Pleistocene series

**Table 3** Statistics of the coseismic landslides and debris flows in Jiuzhaigou County and in the study area

| Investigation region | Investigation area ($km^2$) | Coseismic geohazard | Disaster number | Disaster volume ($\times 10^6 m^3$) | Maximum disaster volume ($m^3$) | Minimum disaster volume ($m^3$) | Average disaster volume ($m^3$) | Total disaster volume ($\times 10^6 m^3$) |
|---|---|---|---|---|---|---|---|---|
| Jiuzhaigou County | 5286 | Landslide | 5478 | 36.09 | 4779655 | 1 | 6588 | 44.16 |
| | | Debris flow | 134 | 8.07 | 472258 | 2598 | 60224 | |
| Study area | 939 | Landslide | 5431 | 34.76 | 4779655 | 1 | 6400 | 42.61 |
| | | Debris flow | 132 | 7.85 | 472258 | 2598 | 59470 | |

precipitation also played an important causative role in the Jiuzhaigou coseismic landslides and debris flows.

Within 1 year after the earthquake, 951 geohazards had newly occurred in the study area with a gross volume of $23.05\times10^6 m^3$, consisting of 756 landslides over $6.4\times10^6 m^3$ and 195 debris flows over $16.65\times10^6 m^3$. The new landslides were dominantly (98.81%) characterized by small sizes and only occupied 27.77% of the total volume of the new PSLDs, whereas the dramatically increased debris flows accounted for 72.23% of the total volume. Coseismic geohazards provided ample source materials, and elevated rainfall was the leading trigger for the new hazards in 2018; thus, the new PSLDs prevailed in the regions with intensive coseismic hazards and sufficient rainfall. The region enriched in rainfall, with accumulation rainfall larger than 840 mm from August 2017 to July 2018, was typical of 94.05% of new landslides and 95.38% of new debris flows (Figure 2b). Therefore, significantly increased debris flow activities, associated with the enhanced rainfall, in the coseismic-hazard-concentrated area were the distinctive PSLD characteristic within 1 year after the earthquake.

During the second year after the earthquake, the number and area of new landslides and debris flows both significantly decreased. Only 31 new geohazards emerged in the study area covering $2.41 \times 10^6 m^3$, composed of 16 landslides covering $0.61\times10^6 m^3$ and 15 debris flows covering $1.80\times10^6 m^3$, concentrated around roads or in bare lands (Figure 2c). Debris flow activities were still a dominant phenomenon, accounting for 74.69% of the total volume of the new PSLDs. Because the average cumulative rainfall (610 mm) during the second year

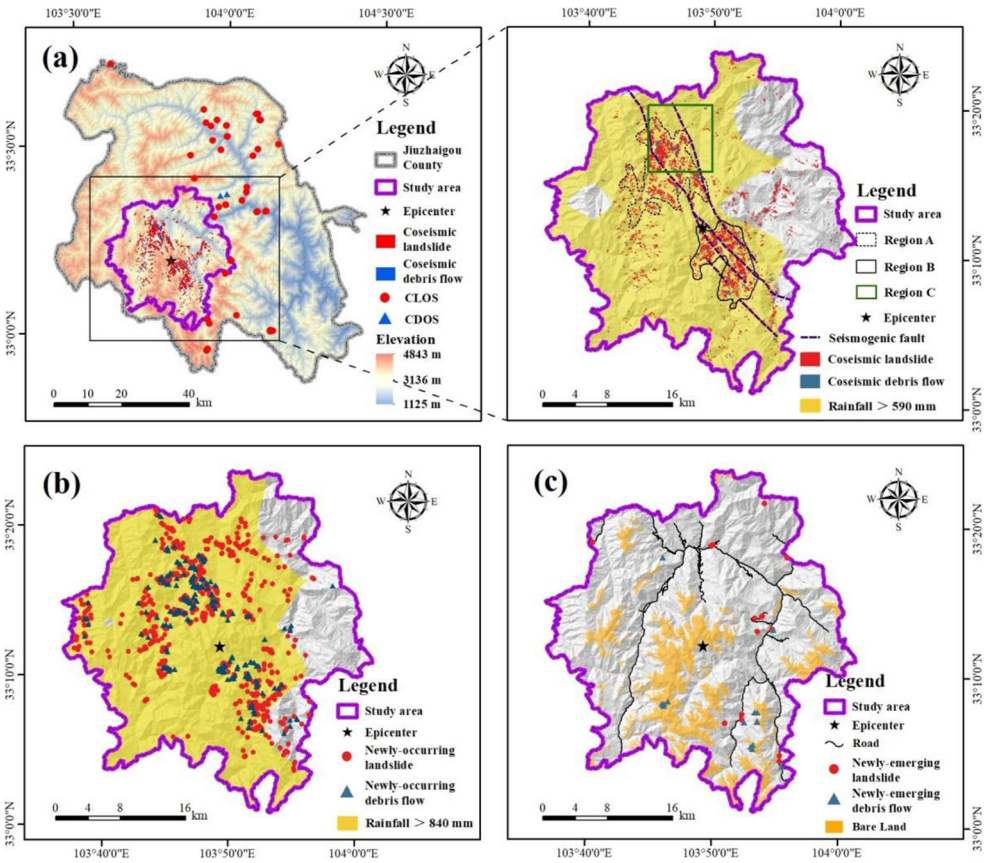


**Figure 2** Geohazard distribution maps in Jiuzhaigou County and in the study area. **a** Distribution of the coseismic landslides and debris flows in 2017. **b** Distribution of the newly occurring landslides and debris flows in 2018. **c** Distribution of the newly emerging landslides and debris flows in 2019. CLOS, coseismic landslides outside of the study area; CDOS, coseismic debris flows outside of the study area

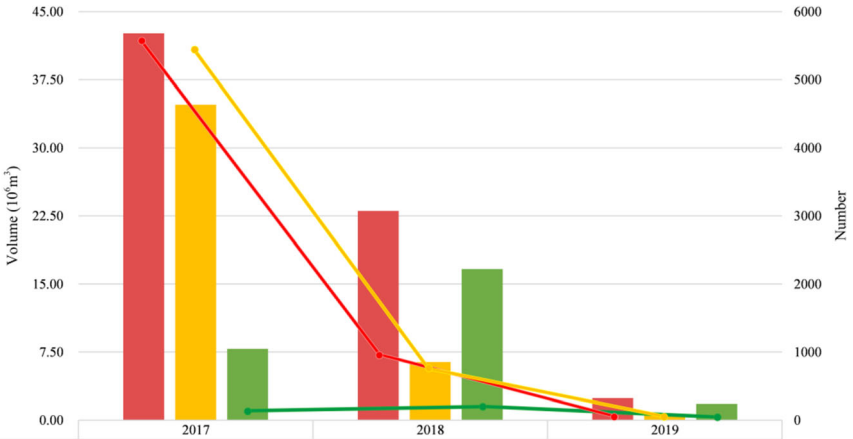


| | 2017 | 2018 | 2019 |
|---|---|---|---|
| Disaster volume ($10^6m^3$) | 42.61 | 23.05 | 2.41 |
| Landslide volume ($10^6m^3$) | 34.76 | 6.40 | 0.61 |
| Debris flow volume ($10^6m^3$) | 7.85 | 16.65 | 1.80 |
| Disaster number | 5563 | 951 | 31 |
| Landslide number | 5431 | 756 | 16 |
| Debris flow number | 132 | 195 | 15 |
| Maximum disaster volume ($m^3$) | 4779655 | 948422 | 492014 |
| Minimum disaster volume ($m^3$) | 1 | 29 | 119 |
| Average disaster volume ($m^3$) | 7660 | 24238 | 77742 |

**Figure 3** Geohazard statistics in the study area from 2017 to 2019. The geohazards in 2017 refer to the coseismic hazards, and the disasters in 2018 and 2019 indicate the newly occurring ones

was lower than the average (851 mm) during the first year, the significant mitigation of hazard activities highlights the evolution trend to a new balance in the absence of rainstorm events.

Furthermore, loose deposits generated by the coseismic and post-seismic landslides and debris flows are illuminated in distribution, transition, and mass wasting in the supplementary file. Both field survey and remote sensing technique show that loose deposits significantly reduced within 2 years after the earthquake. The sustained consumption of loose deposits and the prominent reduction in new sediments indicate that the geological environment was gradually restoring. (Refer to the supplementary file for the detailed loose deposit investigation and mass wasting rule.)

## Evolution of post-seismic landslides and debris flows

The developments of landslides and debris flows after the earthquake are shown in Figures 5, 6, and 7 and Figure S8 in the supplementary file. During the first post-seismic year, 50.87% of the 5431 coseismic landslides in the study area remained active, accompanied by mass wasting and new loose deposits, with the volume increasing from $16.51\times10^6m^3$ in 2017 to $21.31\times10^6m^3$ in 2018. 47.76% of the coseismic

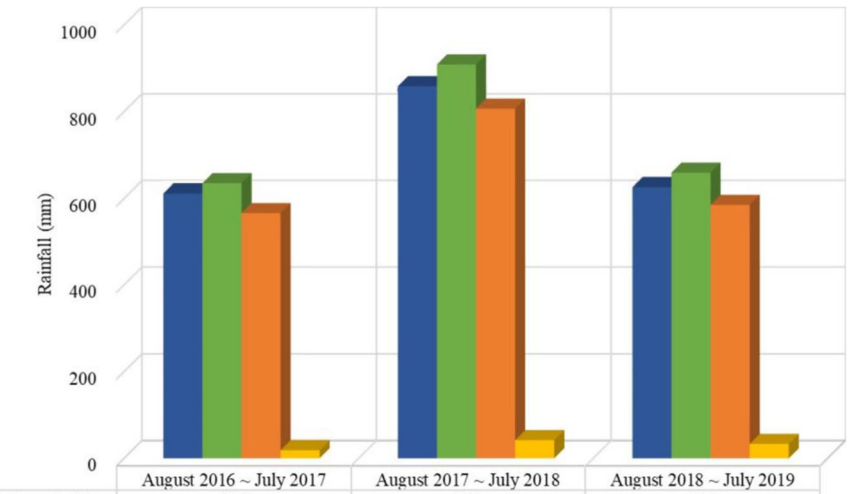


| | August 2016 ~ July 2017 | August 2017 ~ July 2018 | August 2018 ~ July 2019 |
|---|---|---|---|
| Average cumulative rainfall | 596 mm | 851 mm | 610 mm |
| Maximum cumulative rainfall | 619 mm | 901 mm | 643 mm |
| Minimum cumulative rainfall | 550 mm | 795 mm | 570 mm |
| MCR | 19 mm | 42 mm | 33 mm |

**Figure 4** Rainfall statistics from 2017 to 2019 in the study area. The cumulative rainfall in 2017, 2018, and 2019 signifies the accumulative rainfall from August 2016 to July 2017, from August 2017 to July 2018, and from August 2018 to July 2019, respectively. Each continuous precipitation event corresponds to a cumulative rainfall value, and the abbreviation of MCR implies the maximum cumulative rainfall among all the continuous precipitation events

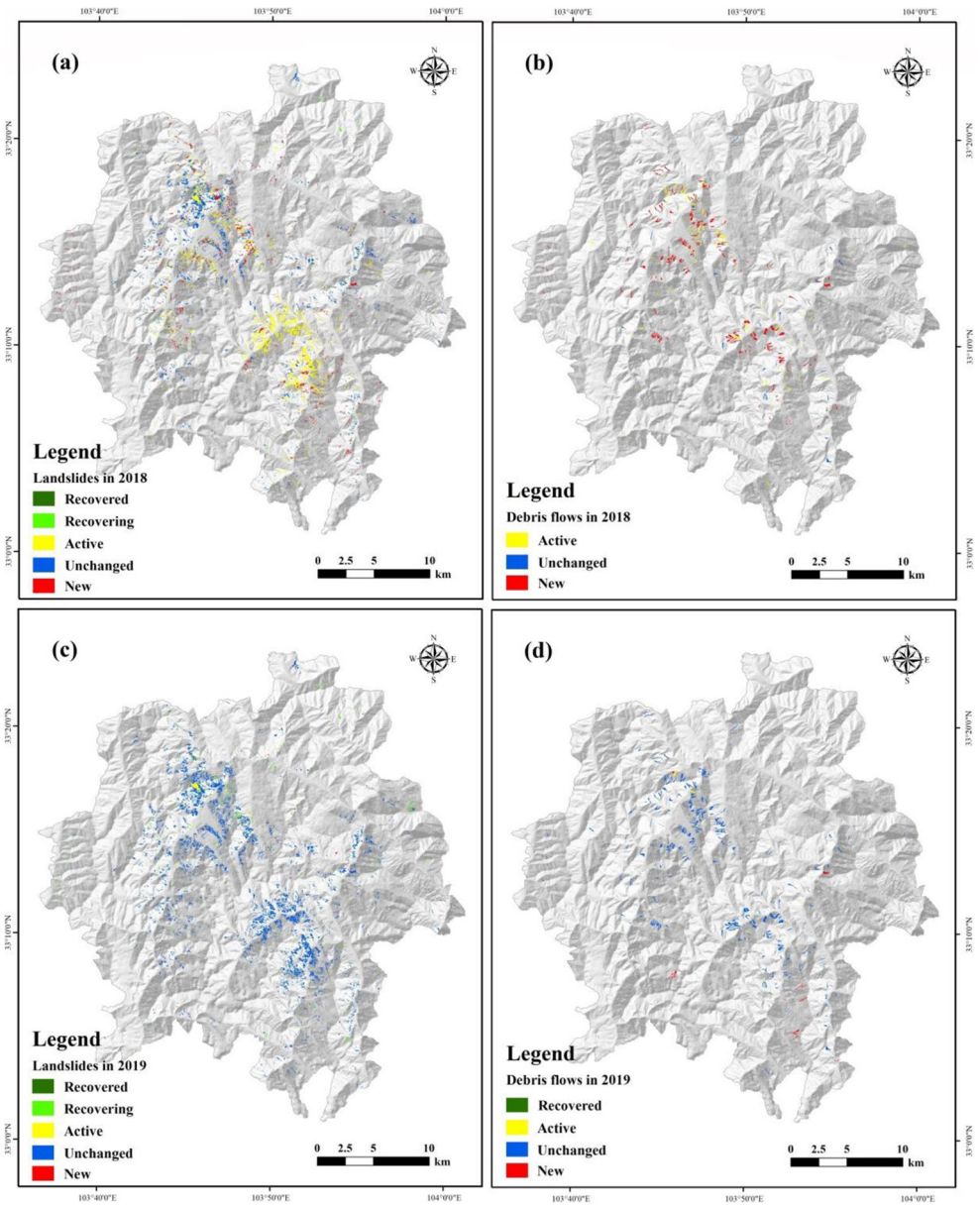


**Figure 5** **a**–**d** Distribution maps of various geohazard (landslide and debris flow) evolution classes in 2018 and 2019

landslides remained unchanged and unvegetated covering $13.21\times10^6m^3$, 1.34% were undergoing recovery and were partly vegetated, and only 1 coseismic landslide was completely vegetated. The average cumulative rainfall across the study area rose from 596 mm before the earthquake to 851 mm in 2018; thus, mainly under the actions of earthquake-loosened slopes and enhanced rainfall, 756 landslides newly appeared covering $6.40\times10^6m^3$.

Over the first year, among the 132 coseismic debris flows, 71.97% dynamically progressed or resurged, together with additional source materials, and extended from a volume of $4.44\times10^6m^3$ in 2017 to $6.58\times10^6m^3$ in 2018. 28.03% stayed inactive and unvegetated covering $2.75\times10^6m^3$, and no coseismic debris flow recovered and experienced good vegetation growth. The debris flow activity was significantly aggravated within the first year, and 195 new events occurred, accounting for 59.63% of the post-seismic debris flows (PSDFs).

Within the second year, the number of active landslides dramatically decreased from 2763 in 2018 to 45 in 2019, occupying only 0.73% of the post-seismic landslides (PSLs), covering $5.03\times10^6m^3$. The new landslides also significantly reduced from 756 in 2018 to 16 in 2019, making up 0.26% of the PSLs, covering $0.61\times10^6m^3$. The recovered and recovering landslides obviously increased from 74 in 2018 to 538 in 2019, constituting 8.68% of the PSLs, and the unchanged landslides without vegetation coverage also distinctly grew from 2594 in 2018 to 5604 in 2019, accounting for 90.34% of the PSLs covering $34.15\times10^6m^3$.

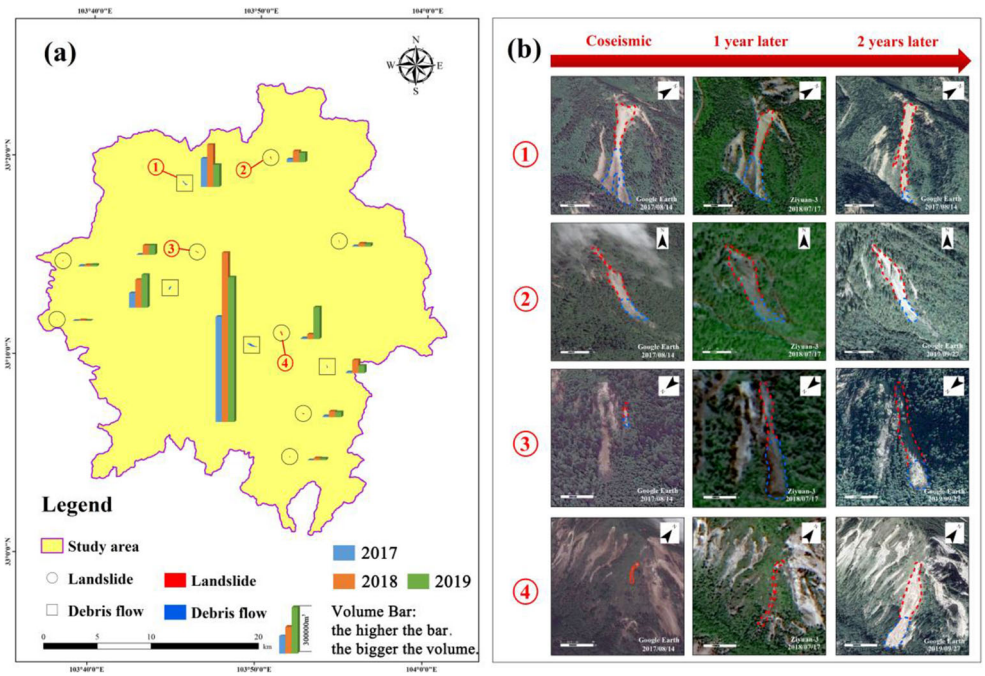


**Figure 6** Evolution characteristics of some representative landslides and debris flow. **a** Evolution histograms. **b** Evolution images of four selected geohazards

In the second year, debris flows exhibited a variation tendency similar to landslides. The active debris flows clearly dropped from 95 in 2018 to 6 in 2019, making up 1.75% of the PSDFs, covering $0.54\times10^6 m^3$. Also, the new debris flows dramatically declined from 195 in 2018 to 15 in 2019, accounting for 4.39% of the PSDFs, covering $1.80\times10^6 m^3$. In contrast, the recovered debris flows increased from 0 in 2018 to 11 in 2019, comprising 3.22% of the PSDFs and covering $0.14\times10^6 m^3$. The unchanged debris flows soared from 37 in 2018 to 310 in 2019, comprising 90.64% of the PSDFs and covering $25.39\times10^6 m^3$.

Therefore, over the first year, the PSLDs remained intense and developed. Most PSLDs, especially debris flows, stayed moving with enlarged areas, newly generated deposits, and mass wasting. Few PSLDs were recovering and only one PSLD was basically recovered. Moreover, the intensification of debris flow activity was another significant characteristic, and debris flows became an important hazard after the earthquake. Although the number of new debris flows was much lower than that of new landslides, the volume of new debris flows was 2.6 times the volume of new landslides. The volumes of new debris flows and new landslides accounted for

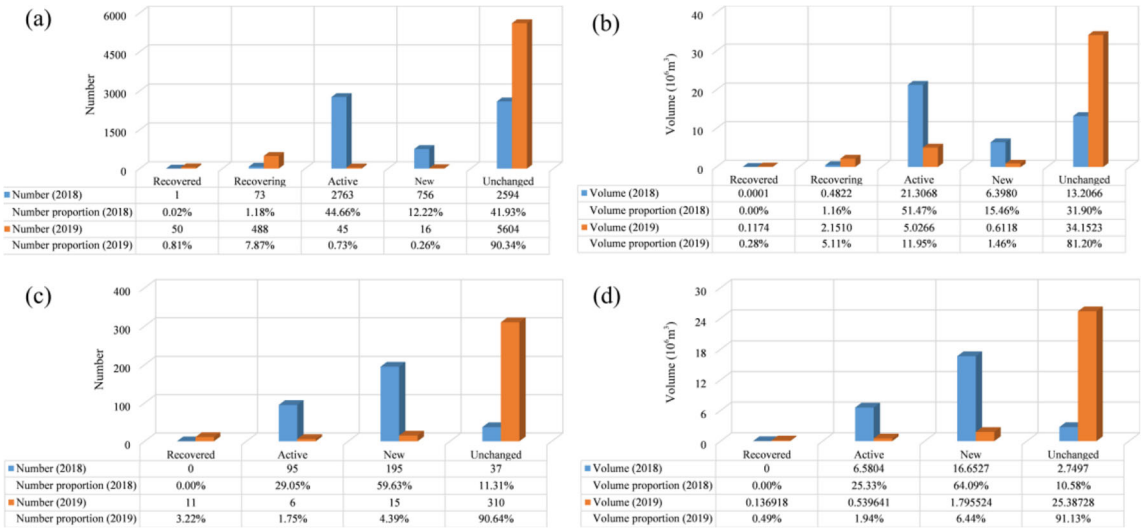


**Figure 7** Statistics of various evolution classes in 2018 and 2019. **a** Statistics of landslide evolution in number and number proportion. **b** Statistics of landslide evolution in volume and volume proportion. **c** Statistics of debris flow development in number and number proportion. **d** Statistics of debris flow development in volume and volume proportion

24.72% and 9.5% of the total PSLD volume, respectively. The enhanced rainfall in the first year may have to a certain degree facilitated the PSLD activity.

The PSLD evolution within the second year is in sharp contrast to the development in the first year. Both the active and new PSLDs dramatically reduced in number and volume, occupying a small portion of the PSLDs. Meanwhile, the recovering and recovered PSLDs significantly increased in number and volume. The vast majority of the PSLDs remained unchanged and unvegetated, and the unvaried ones attained 90.36% of the PSLDs in quantity ratio and 85.16% in proportional volume. Furthermore, recovery from debris flows was evidently slower than that from landslides. The number of restoring and restored landslides was 8.82 times the number of active and new landslides, whereas the number of restored debris flows was only 52.38% of the number of active and new debris flows. The restoring and restored landslides and the recovered debris flows accounted for 8.22% and 0.17% of the PSLDs in number, respectively, and comprised 3.24% and 0.2% of the PSLDs in volume, respectively. Accompanied by the decreased rainfall from an average of 851 mm in 2018 to 610 mm in 2019, the trends are obvious for the self-healing of the geological environment and hazard mitigation. Therefore, the geological environment was rapidly recovering in the absence of extreme rainfall events.

Furthermore, the geohazard chains in the 2 years mainly include (1) evolution from landslides to debris flows and (2) lake-level uplift and dam break soon after the earthquake. (See the supplementary file for the concrete illumination of the geohazard chains.)

## Discussions

### Relationship between geohazard evolution and influencing factors

The maps of various influencing factors are shown in Figures S10 and S11 in the supplementary file, and the relationships between geohazard evolution and influencing factors are shown in Figures S12–S14 in the supplementary file and Figures 8 and 9. The road network and river system remained almost unchanged during the 2 years after the earthquake. Among the influencing factors, only 12 factors played important roles in landslide and debris flow evolution, including distance to seismogenic fault, distance to epicenter, PGA, seismic intensity, fault density, distance to fault, aspect, NDVI, distance to river, cumulative rainfall, distance to road, and land use. Therefore, the PSLD evolution is controlled or induced by the antecedent earthquake, fault tectonics, topography, vegetation growth, hydrology, precipitation, and human engineering activity.

#### Recovering and recovered geohazards and influencing factors

The important factors influencing PSLD recovery included distance to seismogenic fault, distance to epicenter, PGA, seismic intensity, fault density, distance to fault, distance to river, NDVI, cumulative rainfall, and distance to road. Thus, the anterior earthquake, fault tectonics, hydrology, vegetation growth, precipitation, and human engineering activity

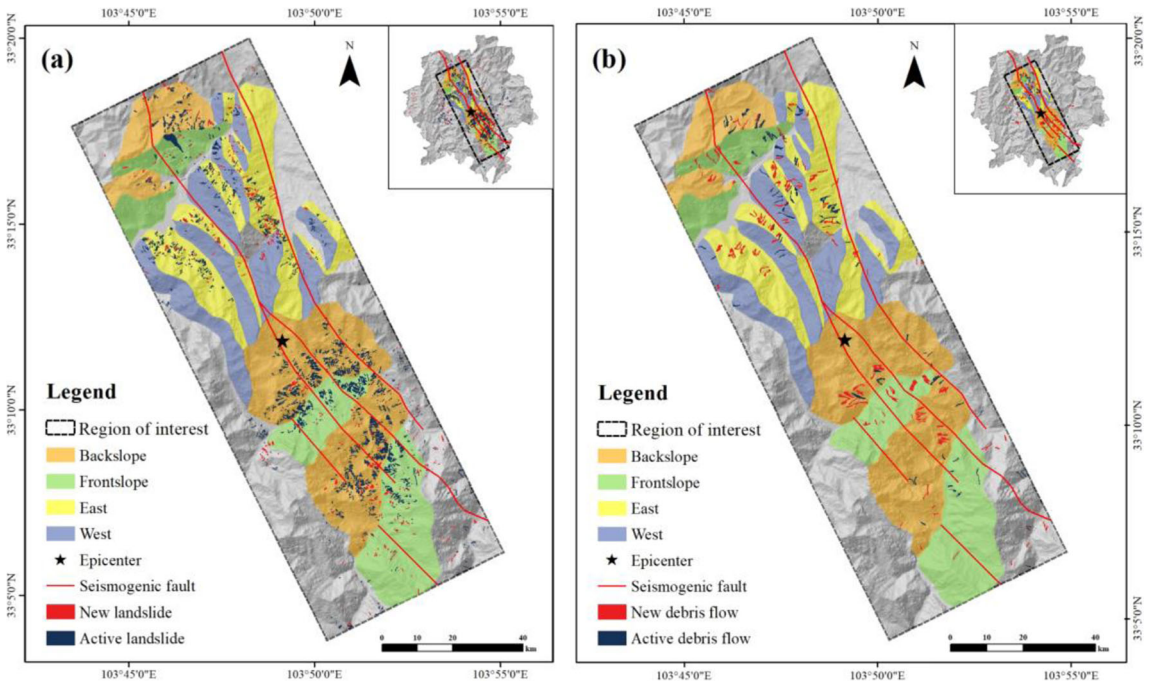


**Figure 8** Aspect effects on the active and new landslides and debris flows in 2018. **a** Back-slope and east-slope effects on the active and new landslides. **b** Back-slope and east-slope effects on the active and new debris flows

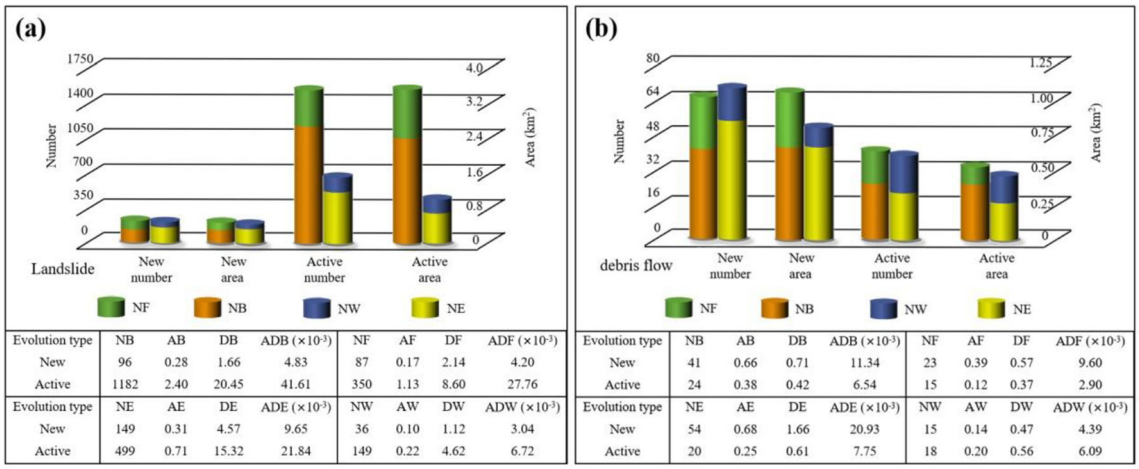


| Evolution type | NB | AB | DB | ADB (×10⁻³) | NF | AF | DF | ADF (×10⁻³) |
|---|---|---|---|---|---|---|---|---|
| New | 96 | 0.28 | 1.66 | 4.83 | 87 | 0.17 | 2.14 | 4.20 |
| Active | 1182 | 2.40 | 20.45 | 41.61 | 350 | 1.13 | 8.60 | 27.76 |
| Evolution type | NE | AE | DE | ADE (×10⁻³) | NW | AW | DW | ADW (×10⁻³) |
| New | 149 | 0.31 | 4.57 | 9.65 | 36 | 0.10 | 1.12 | 3.04 |
| Active | 499 | 0.71 | 15.32 | 21.84 | 149 | 0.22 | 4.62 | 6.72 |

| Evolution type | NB | AB | DB | ADB (×10⁻³) | NF | AF | DF | ADF (×10⁻³) |
|---|---|---|---|---|---|---|---|---|
| New | 41 | 0.66 | 0.71 | 11.34 | 23 | 0.39 | 0.57 | 9.60 |
| Active | 24 | 0.38 | 0.42 | 6.54 | 15 | 0.12 | 0.37 | 2.90 |
| Evolution type | NE | AE | DE | ADE (×10⁻³) | NW | AW | DW | ADW (×10⁻³) |
| New | 54 | 0.68 | 1.66 | 20.93 | 15 | 0.14 | 0.47 | 4.39 |
| Active | 20 | 0.25 | 0.61 | 7.75 | 18 | 0.20 | 0.56 | 6.09 |

**Figure 9** Statistics of the aspect effects on the active and new landslides and debris flows in 2018. **a** Statistics of the back-slope and east-slope effects on the active and new landslides. **b** Statistics of the back-slope and east-slope effects on the active and new debris flows. The abbreviations of NB, AB, DB, and ADB mean the number, area, number density, and area density of the geohazards on the back slopes, respectively. The abbreviations of NF, AF, DF, and ADF represent the number, area, number density, and area density of the geohazards on the front slopes, respectively. The abbreviations of NE, AE, DE, and ADE indicate the number, area, number density, and area density of the geohazards on the eastern slopes, respectively. The abbreviations of NW, AW, DW, and ADW signify the number, area, number density, and area density of the geohazards on the western slopes, respectively

controlled or induced the restoration of PSLDs. There are three characteristics of PSLD recovery. First, the PSLDs, which were less influenced by the earthquake and fault development and far away from rivers and roads, more easily resumed to a new balance. Second, the geological environment and precipitation condition conducive to vegetation growth were beneficial to PSLD restoration. Vegetation development provided a good capacity for soil and water conservation, reinforced the slope stability (Swanson and Dryness 1975; Woo and Luk, 1990; Sidle and Ochiai 2006), and contributed to PSLD recovery. Third, the newly emerging geohazards after the earthquake were more inclined to resume than the coseismic hazards. The influencing factors and the three characteristics are specifically highlighted in the supplementary file.

### Active geohazards and influencing factors

The dominant factors for active PSLDs included distance to seismogenic fault, seismic intensity, distance to fault, fault density, aspect, distance to road, distance to river, and precipitation. Therefore, the anterior earthquake, fault tectonics, topography, road construction, river system, and precipitation led to active PSLDs. There are three distribution features of active PSLDs. First, the active PSLDs primarily appeared in the areas relatively close to faults, roads, and rivers and with abundant rainfall. Compared with the first year, in the second year, the influences of human engineering activity and river erosion intensified, and the active PSLDs that were impacted by human engineering activity and river development increased in quantity proportion. Second, the back-slope effect (Xu and Li 2010) was obvious for the active PSLDs, especially for the active landslides in the first year after the earthquake (Figures 8 and 9). Seismic waves propagated from northwest to southeast (CENC 2017; Li et al. 2017), and the active landslides relatively clustered on the slopes nearly perpendicular to the seismogenic fault and backing to the seismic wave propagation. Third, the east-slope (and southeast-slope) effect was interesting for the active PSLDs in the first year (Figures 8 and 9). Some ridges were almost parallel to the seismogenic fault or intersected the seismogenic fault at small angles. Active PSLDs were relatively concentrated on the east-facing slopes of the ridges. The dominant aspects of the back slope and east slope may have been due to stress enlargement when seismic waves were compressed and multiplicatively reflected from the free surfaces of the back and eastern slopes, which caused slope spalling, shattering, and relaxing (Tang et al. 2009; Xu and Li 2010). Tension cracks and failure planes tended to occur in the superficial rock mass of the back and eastern slopes (Tang 1997; Sang et al. 2003). Moreover, the seismogenic fault was dominated by a NW-SE-oriented left-lateral strike-slip movement (CENC 2017; Li et al. 2017; Yi et al., ..), and the left-lateral mechanism may have influenced the refraction and reflection of the seismic waves between the eastern slope surfaces and the internal slopes and may have been involved with the eastern slope shattering (Wang et al. 2018). Slope relaxation led to instability of the back and eastern slopes and made them tend to become active hazards within a short period after the earthquake. The dominant controlling and triggering factors and the distribution characteristics of active PSLDs are concretely elucidated in the supplementary file.

### New geohazards and influencing factors

There are two types of new geohazards. The first type is the re-sliding of the loose body on the original landslides or debris flows to form a new large landslide or debris flow. The second type is newly emerging landslides and debris flows independent of the re-sliding of the original loose deposits. The first type was closely associated with the distribution of coseismic landslides and debris flows and concentrated in the areas with dense coseismic geohazards. Regarding the second type, the critical factors for the new PSLDs included distance to the seismogenic fault, seismic intensity, PGA, fault density, distance to fault, aspect, distance to river, distance to road, land use, and rainfall. Thus, the antecedent earthquake, fault tectonics, topography, river system, human engineering activity, and precipitation controlled or triggered the occurrence of the second type of new PSLDs. There are three distribution characteristics of the second type of new PSLDs. First, in the first year, abundant rainfall played an important role in newly occurring PSLDs, and new PSLDs also tended to appear near faults. Human engineering activity and river development to some degree contributed to the new emergence of PSLDs. Second, within the second year, human engineering activity, for example, road construction and land use, had an important influence on newly emerging PSLDs. The new PSLDs were mainly triggered by human engineering activity. Third, the distribution of new PSLDs (including the two types) in the first year was not evidently controlled by the back-slope effect but was greatly affected by the east-slope effect (Figures 8 and 9). New PSLDs were relatively concentrated on the eastern slopes of the ridges parallel to the seismogenic fault or intersecting the seismic fault at small angles. Thus, the stress difference between the eastern and western slopes caused by the seismic waves was relatively large, which resulted in the difference of the slope-loosened degrees and then led to the difference in PSLD occurrence levels. The critical influencing factors and distribution features of new PSLDs are specifically clarified in the supplementary file.

## Comparison with some earthquake events

Certain earthquake events, for which PSLD evolution and coseismic geohazard magnitudes were specifically investigated in the previous works, are selected for comparison with the Jiuzhaigou earthquake (Tables 4 and 5).

For fault characteristics, the Jiuzhaigou earthquake was triggered by a blind left-lateral strike-slip fault (CENC 2017; Li et al. 2017; Yi et al., 2017), whereas the other earthquakes in Table 5 are induced mainly by thrust or reverse faults (Berryman 1980; Lee et al. 2001; Sato et al. 2007; Zhao and Xu 2008; Kargel et al. 2016; Xu 2018). A reverse (including thrust) earthquake results in significantly stronger surface damage than a strike-slip earthquake of similar magnitude (Xu 2018). Moreover, four of these thrust or reverse earthquakes caused surface rupture or surface displacement (Henderson 1937; Lin et al. 2006; Zhao and Xu 2008; Kaneda et al. 2008). However, there was no obvious fault fracture or trace generated during the Jiuzhaigou earthquake (CENC 2017; Xu et al. 2017; Yi et al. 2017). Therefore, there was no obvious damage caused by the Jiuzhaigou earthquake to the Earth's surface, and the destruction was less than that of the other five earthquakes.

With regard to coseismic hazard magnitudes, because of the strike-slip focal mechanism (Xu et al. 2017; Yi et al. 2017, ..) and no obvious surface rupture (Fan et al. 2018), the geohazards triggered by the Jiuzhaigou earthquake were dominated by small scales and shallow depths; thus, they possessed much smaller areas and volumes than those caused by the five thrust or reverse earthquakes (Berryman 1980; Lee et al. 2001; Sato et al. 2007; Zhao and Xu 2008; Kargel et al. 2016; Xu 2018). The landslide volumes triggered by the four earthquakes (Gorkha, Wenchuan, Kashmir, and Chi-Chi) were 22–272 times the volume induced by the Jiuzhaigou earthquake, and the landslide area resulting from the Murchison earthquake was nearly 18 times the area caused by the Jiuzhaigou earthquake. Therefore, the loose deposits generated by the Jiuzhaigou earthquake should be much less voluminous than the sediments generated by the other five earthquakes.

For rainfall, Jiuzhaigou County is characterized by a plateau monsoon climate (Gu 2019) with relatively low rainfall. The rainfall in Jiuzhaigou County is significantly less than that in the affected areas of the Gorkha, Kashmir, and Chi-Chi earthquakes. The average annual rainfall in the earthquake-influenced areas of Gorkha, Kashmir, and Chi-Chi is nearly 3 times, 2 times, and over 3 times the mean annual rainfall in Jiuzhaigou County, respectively. Although the rainfall in Jiuzhaigou County is similar to that in the partially affected area of the Wenchuan earthquake, the fault generated during the Wenchuan earthquake propagated approximately 240 km from the epicenter (Chen 2008; Zhao and Xu 2008), and the coseismic landslide volume triggered by the Wenchuan earthquake was over 272 times the volume caused by the Jiuzhaigou earthquake.

For the recovery period, the landslide activities following the Kashmir and Chi-Chi earthquakes quickly returned to equilibrium and the landscapes resumed new stabilities within 2 to approximately 6 years after the earthquakes (Saba et al. 2010; Khattak et al. 2010; Hovius et al. 2011; Khan et al. 2013; Shafique 2020). In contrast, the landslide and debris flow activity after the Wenchuan earthquake may be restored to pre-earthquake levels within two decades (Yang et al. 2018a) or even longer under the action of extreme rainfall (Li et al. 2018), due to enormous landslides (Xu et al. 2016a), extremely large rock avalanches (Xu et al. 2014; Fan et al. 2018), and massive destruction to the geological

**Table 4** Comparison of coseismic hazard magnitudes in five earthquake events. The earthquake magnitudes of the Jiuzhaigou, Gorkha, and Wenchuan earthquakes are from the National Aeronautics and Space Administration and China Earthquake Administration. The earthquake magnitudes of the Kashmir and Murchison earthquakes are from Xu (2015). The $M_w$ and $M_s$ values of the Chi-Chi earthquake are from National Aeronautics and Space Administration and Xu (2015)

| Earthquake | Date | $M_w$ | $M_s$ | Investigation area ($km^2$) | Disaster number | Disaster area ($km^2$) | Disaster volume ($\times 10^6$ $m^3$) | Mean area ($m^2$) | Mean volume ($m^3$) | References |
|---|---|---|---|---|---|---|---|---|---|---|
| Jiuzhaigou earthquake | 08 August 2017 | 6.5 | 7.0 | 840 | 1883 | 8.11 | 25–30 | 4307.00 | 13277–15932 | Fan et al. 2018 |
| | | | | -- | >4800 | 9.60 | -- | 2000.00 | -- | Xu et al., 2018 |
| | | | | 1275 | 2212 | 11.80 | -- | 5312.90 | -- | Wu et al., 2018 |
| | | | | 434 | 4834 | 9.64 | 80.4 | 1993.40 | 16632.19 | Tian et al. 2019 |
| | | | | 5286 | 5612 | 11.12 | 44.16 | 1968.96 | 7868.85 | This work |
| Gorkha earthquake | 25 April 2015 | 7.8 | 8.1 | 35700 | 47200 | 110 | 964 | 2330.51 | 20423.73 | Xu et al., 2018 |
| Wenchuan earthquake | 12 May 2008 | 7.9 | 8.0 | 110000 | 197481 | 1160 | >12000 | 5873.98 | > 60765.34 | Xu et al. 2016b |
| Kashmir earthquake | 08 October 2005 | 7.6 | 7.7 | 2550 | 2252 | 61 | 1600 | 27087.03 | 546075.09 | (1) Disaster number and area: Kamp et al. 2008; (2) Disaster volume: Tian et al. 2020 |
| Chi-Chi earthquake | 20 September 1999 | 7.6 | 7.3 | -- | 26000 | 159 | 2270 | 6115.38 | 244823.12 | (1) Disaster number and area: Xu et al., 2018; (2) Disaster volume: Tian et al. 2020 |
| Murchison earthquake | 17 June 1929 | 7.7 | 7.8 | 5000 | >7400 | 200 | -- | 27027.03 | -- | Xu et al. 2014 |
| | | | | 92 | >410 | -- | >38 | -- | 92683 | Pearce and Watson 1986 |

**Table 5** Comparison of fault characteristic, precipitation, and recovery period of geological environment in five earthquake events

| Earthquake | Fault | Precipitation (mm) | Recovery period | References |
|---|---|---|---|---|
| 2017 Jiuzhaigou | Blind strike-strip | (1) Pre-earthquake: 595.62<br>(2) The first post-seismic year: 851.00<br>(3) The second post-seismic year: 610.10 | Shorter than the following earthquakes | (1) Fault: Xu et al. 2017; Yi et al., 2017 |
| 2015 Gorkha | Blind thrust | (1) Annual rainfall: 1000 to >3000<br>(2) Annual rainfall in most seismic areas: up to 2000 | More than 3 years | (1) Fault: Kargel et al. 2016<br>(2) Precipitation: Tian et al. 2020<br>(3) Recovery period: Tian et al. 2020 |
| 2008 Wenchuan | Thrust-dominant and right-lateral strike-strip movements<br>Fault rupture: about 240 km | (1) Cumulative rainfall from May to September: 583 to 1007 (from 2008 to 2016) | Two decades or longer | (1) Fault: Zhao and Xu 2008<br>(2) Precipitation: Li et al. 2018<br>(3) Recovery period: Yang et al. 2018a; Li et al. 2018 |
| 2005 Kashmir | Thrust<br>Fault rupture: 70 km | (1) Average annual rainfall: 1457<br>(2) Annual rainfall in 2006: 2284 | 2 to 5 years | (1) Fault: Sato et al. 2007; Kaneda et al., 2008<br>(2) Precipitation: Khan et al. 2013<br>(3) Recovery period: Khan et al. 2013; Shafique et al., 2020 |
| 1999 Chi-Chi | Thrust<br>Fault rupture: over 100 km | (1) Annual rainfall in 1999: 1847.7<br>(2) Annual rainfall in 2000: 2076.2<br>(3) Annual rainfall in 2001: 2613.2<br>(4) Average annual rainfall from 1996 to 2001: 2200.2 | About 6 years | (1) Fault: Lee et al. 2001<br>(2) Precipitation: Lin et al. 2006<br>(3) Recovery period: Hovius et al. 2011 |
| 1929 Murchison | Reverse-dominant and sinistral movements<br>Fault trace: 8 km | | Retention of 50~75% sediments more than 50 years | (1) Fault: Henderson 1937; Berryman 1980<br>(2) Recovery period: Pearce and Watson, 1986 |

environment and landscape. Similarly, the landslide evolution following the Murchison earthquake was characterized by the long-term sediment retention after the earthquake (Pearce and Watson 1986). After 50 years of evolution, at least 50 to 75% of the granitic debris still remained in the fourth-order 92-km$^2$ catchment (Pearce and Watson 1986). In addition, within 3 years following the Gorkha earthquake, 56% of the landslides along the two earthquake-affected highways proceeded to deform and expand and may require over 3 years to restore (Tian et al. 2020). For the Jiuzhaigou earthquake, landslide and debris flow activity intensified in the first year after the earthquake. Most geohazards, especially debris flows, dynamically progressed or resurged under enhanced rainfall, accompanied by additional loose deposits, expanded areas, and mass wasting. However, in the second year, the earthquake influence quickly decayed as the rainfall decreased to the pre-earthquake level, and only a small amount of landslides and debris flows stayed moving. The landslide and debris flow evolution in the second year was primarily controlled by fault development and induced by rainfall and human engineering activity, for example, road construction and land use.

Therefore, compared with the above five earthquakes, the Jiuzhaigou earthquake is characterized by a smaller earthquake magnitude, no obvious surface rupture (Fan et al. 2018), much smaller hazard magnitudes, obviously less rainfall, and rapid attenuation of the earthquake influence. Thus, the geohazard activity and landscape after the Jiuzhaigou earthquake may potentially be restored to equilibrium more quickly than after the Kashmir, Chi-Chi, Gorkha, Wenchuan, and Murchison earthquakes.

## Evolution rule and trend of post-seismic landslides and debris flows

The evolution rule and trend of PSLDs are revealed by integrating geohazard investigation, loose deposit investigation, PSLD evolution, influencing factors, and mass wasting analyzed above.

(1) The Jiuzhaigou earthquake triggered 5563 coseismic geohazards in the study area, including 5431 landslides covering $34.76\times10^6$m$^3$ and 132 debris flows covering $7.85\times10^6$m$^3$. Of these coseismic hazards, 97.43% possessed small scales and 2.52% had medium scales. Of the coseismic hazards, 90.87% occurred in the area with relatively abundant anterior rainfall; thus, infiltration of the anterior precipitation and water softening may make the rock mass more prone to instability during a strong earthquake (Sassa et al. 2007; Fan et al. 2019).

(2) The landslide and debris flow activity became aggravated in the first post-earthquake year. The antecedent earthquake shattered and relaxed the slopes (Tang et al. 2009; Xu and Li 2010), and the coseismic landslides and debris flows generated a mass of loose deposits. Moreover, rainfall significantly increased in the first year, and the developed faults caused broken rock mass, benefited rainfall penetration and groundwater seepage, and created favorable tectonic conditions for slope instability (Koukis et al. 2009). In addition, road construction and fluvial scouring eroded slope toes, which reduced the counterpressure of slope feet (Maharaj 1993; Kamp et al. 2008) or caused hydrodynamic pressure via underground water infiltrating, rising, and declining (He et al. 1998; Miao et al. 2014), and then destroyed slope balance. Therefore, the PSLDs intensified within the first year under the joint effect of loosened slopes, sufficient source materials, developed faults, enhanced rainfall, anterior road construction, and river erosion. However, human engineering activity and river erosion contributed less to the PSLDs than the anterior earthquake, fault tectonics, and precipitation. Most PSLDs stayed moving, highlighted by active and newly emerging landslides and debris flows, accompanied by enlarged areas, newly generated sediments, and mass wasting. A handful of PSLDs were undergoing recovery, and only one landslide was restored.

(3) Landslide and debris flow activity quickly decayed in the second year and may continue several years before returning to a new balance. Driven by gravity and water erosion (Lin et al. 2008; Zhang and Zhang 2017), loose deposits were transported from high altitude to low elevation, and a few were delivered into rivers and lakes. The dissipative deposits were much abundant than the newly generated deposits; thus, the sediments dramatically reduced with time. In the second year, rainfall reduced to the pre-earthquake level, and slopes experienced self-healing by grain coarsening, material consolidation, and vegetation growth (Fan et al. 2018). Therefore, PSLDs rapidly resumed in the second year because of dramatically reduced sediments, decreased rainfall, and self-healing slopes. The recovering and recovered PSLDs significantly increased, and the vast majority of the PSLDs remained inactive. However, the anterior earthquake, fault tectonics, human engineering activity, and meteorology have far-reaching influences on PSLD evolution, and a few PSLDs remained active or newly appeared under the combined action of earthquake-relaxed slopes, fault development, road construction, bare soils and rocks, and rainfall. Moreover, over 90% of the PSLDs remained unchanged and unvegetated and may present two trends in the future. One trend is that without extreme rainfall events, these geohazards may gradually recover and be vegetated, and the sediments may consolidate as part of the landscape (Fan et al. 2019). The other is that in rainstorm events, these geohazards constitute important hidden dangers

and may become active again and generate numerous loose deposits. Although the PSLDs were rapidly decaying and the geological environment was promptly restoring, the geological environment and landscape had not returned to the pre-earthquake levels, because the unrecovered geohazards were still quite significant both in number and volume ($69.66\times10^6$ $m^3$), and abundant sediments still remained on hillslopes or in channels 2 years after the earthquake.

(4) Intensified debris flow activity was a prominent feature shortly after the earthquake. In the first year, 71.97% of the coseismic debris flows remained active, and the newly emerging debris flows dominated the new geohazard activity, mainly due to the rising rainfall and sufficient source materials. No coseismic debris flow recovered in the first year. In the second year, the activity of debris flows dramatically reduced with small amounts of active and new debris flows; however, debris flow activities were still prominent and occupied 74.59% of the total volume of the new PSLDs. Moreover, over 90% of the debris flows remained unchanged and unvegetated and may become hidden dangers in the future when experiencing heavy rains. In addition, debris flows were restored more slowly than landslides, and the number of the restored debris flows was only half of that of the active and new debris flows in the second year.

(5) The geohazard chains within the 2 post-seismic years mainly consisted of (1) evolution from landslides to debris flows and (2) lake-level uplift and dam break soon after the earthquake. Except for chain (2) that occurred shortly following the earthquake, there was no dammed lake generated during the 2 years. With regard to development from landslides to debris flows, loose deposits generated by landslides remained on slopes or were transported to channels by gravity and water erosion (Lin et al. 2008; Zhang and Zhang 2017). These loose deposits provided sufficient source materials for debris flows. Under rainfall events, these sediments, carrying other erosion materials and water, rushed down slopes or to ravine mouths, and then hillslope debris flows or channel debris flows occurred (Curry 1966; Griffiths et al. 2004; Chen et al. 2012; Zhang and Zhang 2017). With respect to dam breaks, vast loose deposits generated by the coseismic landslides and debris flows moved into the lakes and raised the water levels together with the action of the earthquake-induced geomorphology change (Yang et al. 2018b). The pressure on the dam walls correspondingly increased, causing dam breaks (Yang et al. 2018b). The dam breaks generally occurred soon after the earthquake; for example, water in Huohua Lake ran dry on August 9, 2017, shortly after the earthquake.

(6) Aspect controls geohazard evolution and distribution within a short period after the earthquake. Some previous works (e.g., Wang et al. 2011; Zhao et al. 2018) indicated that the topography amplification effect on the PGA of seismic waves intensifies on the back slopes; thus, back slopes are inclined to fail more easily, which is called the back-slope effect on coseismic landslides (e.g., Xu and Li 2010; Xu et al. 2011; Wu et al. 2018). In addition, under the integrated influence of fault movement direction and valley orientation, east and southeast were the dominant aspects of the Jiuzhaigou coseismic landslides (Wang et al. 2018). This work reveals that the fractured and loosened rocks on the back, east-facing, and southeast-facing slopes not only influenced the coseismic landslide distribution but also controlled the PSLD evolution and distribution in a short period. The reinforced destruction to the back, east, and southeast slopes was sourced from the coupled effect of topography amplification and fault movement. The slope destruction caused the active and new PSLDs to tend to occur on the slopes on the three aspects. Moreover, it seemed that active landslides were related to both the topography amplification effect and fault movement direction, and new landslides and debris flows were mainly controlled by fault movement direction.

(7) The geological environment and landscape after the Jiuzhaigou earthquake may return to new balances and restore to the pre-earthquake levels more quickly than after the Kashmir, Chi-Chi, Gorkha, Wenchuan, and Murchison earthquakes. The strike-slip focal mechanism and the blind seismic fault of the Jiuzhaigou earthquake did not generate obvious fault fractures or traces on the Earth's surface (Xu et al. 2017; Yi et al. 2017) and restricted the degree of destruction to the surface. The coseismic and post-seismic geohazards were dominated by small scales, and the meteorological conditions were not favorable for geohazard development due to relatively low rainfall. Thus, although the PSLD activity was aggravated accompanied by the enhanced rainfall in the first year, the earthquake influence rapidly decayed in the second year with rainfall declining to the pre-earthquake level. The newly occurring and dynamically expanding landslides and debris flows comprised only 1.25% of the PSLDs in the second year, and these hazards were mainly controlled by fault development and triggered by rainfall and human engineering activity, such as road construction and land use. Therefore, the recovery period of the PSLD activity and landscape in the Jiuzhaigou area may be shorter than previously expected in the absence of extreme rainfall events.

## Conclusions

In this work, the comprehensive investigation of landslide and debris flow evolution after the 2017 $M_s$ 7.0 Jiuzhaigou earthquake is reported. This work focuses on the spatio-temporal evolution of PSLDs under the effects of the earthquake, geology, terrain, precipitation, drainage system, and human engineering activity. The Jiuzhaigou region possesses unique and significant merits in geology, society, and economy, which is characterized by the famous north-south seismic belt in China (Li et al. 2017), the $M_s$ 7.0 strong earthquake (CENC 2017), ultracomplex geological and topographic context (Lei et al. 2018), UNESCO World Natural Heritage Site (UNESCO 1992; Fan et al. 2018), and World Biosphere Reserve (Fan et al. 2018). Thus, the Jiuzhaigou region is selected as the study area in this work. Multisource and multi-temporal data, including seismic, geological, topographic, meteorological, and remote sensing data, are employed to provide new insights into the PSLD distribution, loose deposit distribution, PSLD evolution, influencing factors, hazard chain, and mass wasting in the Jiuzhaigou area from 2017 to 2019. This work may provide new knowledge pertaining to landslide and debris evolution after a strong earthquake and profound impacts of a catastrophic earthquake on geological environment and landscape. Six main conclusions are drawn as follows.

(1) The landslide and debris flow activity became intensified within the first year after the earthquake under the combined effect of loosened slopes, sufficient source materials, developed faults, enhanced rainfall, anterior road construction, and river erosion. Moreover, intensified debris flow activity was a prominent feature shortly after the earthquake due to the rising rainfall and sufficient source materials. Debris flows were restored more slowly than landslides within a short period after the earthquake.

(2) Landslide and debris flow activity quickly decayed in the second year because of dramatically reduced sediments, decreased rainfall, and self-healing slopes. The activity may continue several years before returning to a new balance. The PSLD activity was rapidly decaying and the geological environments were promptly restoring in an evolution trend to a new balance in the absence of rainstorm events. However, the geological environment and landscape had not returned to the pre-earthquake levels because of the vast unrecovered landslides and debris flows covering $69.66\times10^6$ $m^3$ and the remaining loose deposits trapped on hillslopes or in channels. Furthermore, the PSLD activity level may fluctuate and significantly increase in the future when experiencing extreme rainfall events.

(3) The geohazard chains within 2 years after the earthquake mainly consisted of (a) evolution from landslides to debris flows and (b) lake-level uplift and dam break soon after the earthquake.

(4) The earthquake-generated sediments were quickly consumed by water erosion, transport to rivers and lakes, and artificial removal. The sustained and rapid consumption of coseismic loose deposits and the prominent reduction in new sediments indicate that the geological environment was gradually restoring.

(5) The geological environment and landscape after the Jiuzhaigou earthquake may return to new balances and restore to the pre-earthquake levels more quickly than after the Kashmir, Chi-Chi, Gorkha, Wenchuan, and Murchison earthquakes, as a result of a smaller earthquake magnitude, no obvious surface rupture, much smaller hazard magnitudes, obviously less rainfall, and rapid attenuation of the earthquake influence.

(6) The activity and new emergence of post-earthquake landslides and debris flows are chronically influenced by the anterior earthquake and pre-earthquake human engineering activity (especially road construction) due to the sustained effects of the fractured and loosened rocks and slopes. Therefore, human construction activity has a profound impact on geohazard evolution, and the balance between economic progress and the natural environment should be more carefully considered.

**Supplementary Information** The online version contains supplementary material available at https://doi.org/10.1007/s11356-021-16789-9.

**Acknowledgements** We are much grateful for the valuable comments of Professor Philippe Garrigues and the two anonymous reviewers. These comments have improved the manuscript a lot.

**Availability of data and materials** All data are available within this article and its supplementary material. The datasets used and analyzed during the current study are available from the corresponding author on reasonable request.

**Author contribution** Xianmin Wang: conceptualization, methodology, formal analysis, writing—original draft, writing—review and editing. Hang Mao: formal analysis, investigation, writing—review and editing. All authors read and approved the final manuscript.

**Funding** This work is funded by the Opening Fund of Key Laboratory of Geological Survey and Evaluation of Ministry of Education (Grant No. GLAB2020ZR02), State Key Laboratory of Biogeology and Environmental Geology (Grant No. GBL12107), China University of Geosciences, and the Fundamental Research Funds for the Central Universities.

## Declarations

**Ethics approval and consent to participate** Not applicable.

**Consent for publication** Not applicable.

**Conflict of interest** The authors declare no competing interests.

## References


Avouac JP (2007) Dynamic processes in extensional and expressional settings-mountain building: from earthquake to geological deformation. Treatise Geophysics 6:377–439

Basharat M, Riza MT, Jan MQ et al (2021, online) A review of landslides related to the 2005 Kashmir earthquake: implication and future challenges. Natural Hazards. https://doi.org/10.1007/s11069-021-04688-8

Berryman KR (1980) Late Quaternary movement on White Creek Fault, South Island, New Zealand. New Zealand Journal of Geology and Geophysics 23(1):93–101

Broeckx J, Rossi M, Lijnen K (2020) etc. Landslide mobilization rates: a global analysis and model. Earth-Science Reviews 201:102972

Cao J., Zhang Z., Wang C., etc. Susceptibility assessment of landslides triggered by earthquakes in the Western Sichuan Plateau. Catena, 2019, 175: 63-76.

Cao J, Zhang Z, Du J (2020) etc. Multi-geohazards susceptibility mapping based on machine learning - a case study in Jiuzhaigou, China. Natural Hazards 102:851–871

CENC, China Earthquake Networks Center, China Earthquake Administration. Website: http://www.cenc.ac.cn/. Accessed 11 September 2017.

Chang M, Tang C, Ni H (2015) Evolution process of sediment supply for debris flow occurrence in the Longchi area of Dujiangyan City after the Wenchuan earthquake. Landslides 12(3):611–623

Chang M., Cui P., Xu L., et al. The spatial distribution characteristics of coseismic landslides triggered by the $M_s$ 7.0 Lushan earthquake and $M_s$ 7.0 Jiuzhaigou earthquake in southwest China. Environmental Science and Pollution Research, 2021, online, DOI: https://doi.org/10.1007/s11356-020-11826-5

Chen Y (2008) On the magnitude and fault length of the great Wenchuan earthquake. Science and Technology Review 26(10):26–27

Chen HX, Zhang LM, Chang DS (2012) etc. Mechanics and runout characteristics of the rainfall-triggered debris low in Xiaojiagou in Sichuan Province, China. Natural Hazards 62(3):1037–1057

Chen X, Chen J, Cui P et al (2018) Assessment of prospective hazards resulting from the 2017 earthquake at the world heritage site Jiuzhaigou Valley, Sichuan, China. Journal of Mountain Sciences 15(4):779–792

Chen X, Shan X, Wang M, Liu C, Han N (2020) Distribution pattern of coseismic landslides triggered by the 2017 Jiuzhaigou Ms 7.0 earthquake of China: control of seismic landslide susceptibility. ISPRS Int. J. Geo-Inf 9(4):198. https://doi.org/10.3390/ijgi9040198

Cheng Q, Hu C, Yang X (2018) Developmental regularity and preventive countermeasures of geological hazards along the highway in Jiuzhaigou earthquake area. The Chinese Journal of Geological Hazard and Control 29(4):114–120

Comert R (2021) Investigation of the effect of the dataset size and type in the earthquake-triggered landslides mapping: a case study for the 2018 Hokkaido Iburu landslides. Frontiers in Earth Science 9: 633665

Cui P, Chen XQ, Zhu YY et al (2011) The Wenchuan earthquake (May 12, 2008), Sichuan province, China, and resulting geohazards. Natural Hazards 56(1):19–36

Curry RR (1966) Observations of alpine mudflows in the Tenmile Range, central Colorado. Geol. SOC. Am. Bull. 77:771–776

Dai L, Xu Q, Fan X et al (2017) A preliminary study on spatial distribution pattern of landslides triggered by Jiuzhaigou earthquake in Sichuan on August 8th, 2017 and their susceptibility assessment. Journal of Engineering Geology 25(4):1151–1164

Domènech G, Fan X, Scaringi G et al (2019) Modeling the role of material depletion, grain coarsening and revegetation in debris flow occurrences after the 2008 Wenchuan earthquake. Engineering Geology 250:34–44

Dong X., Xu Q., She J. et al. Preliminary study on the interpretation of geological hazards in Jiuzhaigou based on multi-source remote sensing data. Geomatics and Information Science of Wuhan University, 2019, online, DOI: https://doi.org/10.13203/j.whugis20190076.

Fan X, Hsein JC, Wasowski J et al (2018) What we have learnt from the 2008 Wenchuan Earthquake and its aftermath: a decade of research and challenges. Engineering Geology 241:25–32

Fan RL, Zhang LM, Wang HJ et al (2018a) Evolution of debris flow activities in Gaojiagou Ravine during 2008-2016 after the Wenchuan earthquake. Engineering Geology 235:1–10

Fan X., Scaringi G., Xu Q., etc. Coseismic landslides triggered by the 8th August 2017 $M_s$ 7.0 Jiuzhaigou earthquake (Sichuan, China): factors controlling their spatial distribution and implications for the seismogenic blind fault identification. Landslides, 2018b, 15: 967-983.

Fan X, Scaringi G, Korup O et al (2019) Earthquake-induced chains of geological hazards: pattern, mechanism, and impacts. Review of Geophysics 57:421–503

Fang L, Wu J, Su J (2018) etc. Relocation of mainshock and aftershock sequence of the $M_s$ 7.0 Sichuan Jiuzhaigou earthquake. Chinese Science Bulletin 63:649–662

Faris F, Wang F (2014) Stochastic analysis of rainfall effect on earthquake induced shallow landslide of Tandikat, West Sumatra, Indonesia. Geoenvironmental Disasters 1(1):12

Griffiths PG, Webb RH, Melis TS (2004) Frequency and initiation of debris flows in Grand Cayon, Arizona. Journal of Geophysical Research: Earth Surface 109:F04002

Gu H. Risk assessment of earthquake-induced collapse disaster in Jiuzhaigou scenic area. Chengdu University of Technology, Doctoral dissertation, 2019.

He M, Yao A, Lu C (1998) etc. Study of mechanical functions of underground water in slope rockmass. Chinese Journal of Rock Mechanics and Engineering 17(6):662–666

Henderson J (1937) The west Nelson earthquakes of 1929. N.Z. Journal of Science and Technology 19(2):66–143

Hovius N, Meunier P, Lin C et al (2011) Prolonged seismically induced erosion and the mass balance of a large earthquake. Earth and Planetary Science Letters 304:347–355

Hu X, Hu K, Tang J et al (2019a) Assessment of debris-flow potential dangers in the Jiuzhaigou Valley following the August 8, 2017, Jiuzhaigou earthquake, western China. Engineering Geology 256: 57–66

Hu X, Hu K, Zhang X et al (2019b) Quantitative assessment of the impact of earthquake-induced geohazards on natural landscapes in Jiuzhaigou Valley. Journal of Mountain Science 16(2):441–452

Huang R (2011) After effect of geohazards induced by the Wenchuan earthquake. Journal of Engineering Geology 19(2):145–151

Kamp U, Growley BJ, Khatta GA et al (2008) GIS-based landslide susceptibility mapping for the 2005 Kashmir earthquake region. Geomorphology 101(4):61–642

Kaneda H, Nakata T, Tsutsumi H et al (2008) Surface rupture of the 2005 Kashmir, Pakistan earthquake and its role for active tectonic implications. Bull. Seismol. Soc. Am. 98:521–557

Kargel JS, Leonard GJ, Shugar DH et al (2016) Geomorphic and geologic controls of geohazards induced by Nepal's 2015 Gorkha earthquake. Science 351(6269):8353

Keefer DK (1984) Landslides caused by earthquakes. Geological Society of America Bulletin 95(4):406–421

Khan SF, Kamp U, Owen LA (2013) Documenting five years of landsliding after the 2005 Kashmir earthquake, using repeat photography. Geomorphology 197:45–55

Khattak GA, Owen LA, Kamp U et al (2010) Evolution of earthquake-triggered landslides in the Kashimir Himalaya, northern Pakistan. Geomorphology 115:102–108

Koukis G, Sabatakakis N, Ferentinou M et al (2009) Landslide phenomena related to major fault tectonics: rift zone of Corinth Gulf,

Greece. Bulletin of Engineering Geology and the Environment 68: 215–229

Koukouvelas IK, Piper DJW, Katsonopoulou D et al (2020) Earthquake-triggered landslides and mudflows: was this the wave that engulfed ancient Helike? Holocene 30(12):1653–1668

Lee WHK, Shin TC, Kuo KW et al (2001) CWB free-field strong-motion data from the 21 September Chi-Chi, Taiwan, earthquake. Bulletin of the Seismological Society of America 91:1370–1376

Lei H, Wang X, Hou H et al (2018) The earthquake in Jiuzhaigou County of Northern Sichuan, China on August 8, 2017. Natural Hazards 90: 1021–1030

Li Y, Huang C, Yi S et al (2017) Study on seismic fault and source rupture tectonic dynamic mechanism of Jiuzhaigou $M_s$ 7.0 earthquake. Journal of Engineering Geology 25(4):1141–1150

Li C, Wang M, Liu K (2018) A decadal evolution of landslides and debris flows after the Wenchuan earthquake. Geomorphology 323:1–12

Li X, Ling S, Sun C et al (2019) Integrated rockfall hazard and risk assessment along highways: an example for Jiuzhaigou area after the 2017 Ms 7.0 Jiuzhaigou earthquake, China. Journal of Mountain Science 16(6):1318–1335

Liang J, Pei X, Wen Y et al (2019) Research on development and distribution rules of geohazards in Jiuzhaigou earthquake in 2017. Journal of Natural Disasters 28(5):181–188

Lin CW, Liu SH, Lee SY et al (2006) Impacts of the Chi-Chi earthquake on subsequent rainfall-induced landslides in central Taiwan. Engineering Geology 86:87–101

Lin GW, Chen H, Chen YH (2008) etc. Influence of typhoons and earthquakes on rainfall-induced landslides and suspended sediments discharge. Engineering Geology 97:32–41

Litoseliti A, Koukouvelas IK, Nikolakopoulos KG et al (2020) An event-based inventory approach in landslide hazard assessment: the case of the Skolis Mountain, Northwest Peloponnese, Greece. ISPRS International Journal of Geo-Information 9:457

Liu G, Zhang Y, Zhang S et al (2018a) Analysis on distribution characteristics of secondary geo-hazards before and after Jiuzhaigou earthquake. Journal of Geological Hazards and Environment Preservation 29(3):1–4

Liu J, Mason PJ, Bryant EC (2018b) Regional assessment of geohazard recovery eight years after the $M_w$ 7.9 Wenchuan earthquake: a remote sensing investigation of the Beichuan region. International Journal of Remote Sensing 39(6):1671–1695

Lu T, Zeng H, Luo Y, etc (2012) Monitoring vegetation recovery after China's May 2008 Wenchuan earthquake using Landsat TM time-series data: a case study in Mao County. Ecol. Res. 27(5):955–966

Maharaj RJ (1993) Landslide processes and landslide susceptibility analysis from an upland watershed: a case study from St. Andrew, Jamaica, West Indies. Engineering Geology 34(1):53–79

Malamud BD, Turcotte DL, Guzzetti F et al (2004) Landslides, earthquakes, and erosion. Earth and Planetary Science Letters 229:45–59

Marc O, Hovius N, Meunier P et al (2015) Transient changes of landslide rates after earthquakes. Geology 43:883–886

Miao H, Wang G, Yin K et al (2014) Mechanism of the slow-moving landslides in Jurassic red-strata in the Three Gorges Reservoir, China. Engineering Geology 171(8):59–69

Nakamura H, Tsuchiya S, Inoue K, etc (2000) Sabo against earthquakes. Kokon Shoin, Tokyo, pp 190–220

Papathanassiou G, Valkaniotis S, Ganas A (2021) Spatial patterns, controlling factors, and characteristics of landslides triggered by strike-slip faulting earthquakes: case study of Lefkada island, Greece. Bulletin of Engineering Geology and the Environment 80(5): 3747–3765

Pearce AJ, Watson AJ (1986) Effects of earthquake-induced landslides on sediment budget and transport over a 50-yr period. Geology 14: 52–55

Porta GF, Bebbington M, Xiao X et al (2021) A statistical model for earthquake and/or rainfall triggered landslides. Frontiers in Earth Science 8:605003

Saba SB, van der Meijde M, van der Werff H (2010) Spatiotemporal landslide detection for the 2005 Kashmir earthquake region. Geomorphology 124:17–25

Sang HC, Ogata Y, Kaneko K (2003) Strain-rate dependency of the dynamic tensile strength of rock. Int. J. Rock. Mech. Min. 40:763–777

Sassa K, Fukuoka H, Wang F et al (2007) Landslides induced by a combined effect of earthquake and rainfall. In Progress in landslide science. Springer, Berlin, pp 193–207

Sato HP, Hasegawa H, Fujiwara S et al (2007) Interpretation of landslide distribution triggered by the 2005 Northern Pakistan earthquake using SPOT 5 imagery. Landslides 4:113–122

SBNESD, Statistical bulletin on national economic and social development in Jiuzhaigou County, Sichuan Province in 2016. 2017, Website: http://www.ahmhxc.com/tongjigongbao/7726.html. Accessed 13 July 2017.

Shafique M (2020) Spatial and temporal evolution of co-seismic landslides after the 2005 Kashmir earthquake. Geomorphology 362: 107228

Shen T, Wang Y, Luo Y et al (2019) Seismic response of cracking features in Jubao Mountain during the aftershocks of Jiuzhaigou $M_s$ 7.0 earthquake. Journal of Mountain Sciences 16(11):2532–2547

Sidle RC, Ochiai H (2006) Landslides: processes, prediction, and land use. American Geophysical Union, Washington DC

Sun J, Yue H, Shen Z et al (2018) The 2017 Jiuzhaigou earthquake: a complicated event occurred in a young fault system. Geophysical Research Letters 45:1–11

Swanson FJ, Dryness CT (1975) Impact of clear-cutting and road construction on soil erosion by landslides in Western Cascade range, Oregon. Geology 3:393–396

Tang C (1997) Numerical simulation of progressive rock failure and associated seismicity. Int. J. Rock. Mech. Min. 34:249–261

Tang C., Zuo Y., Qin S., et al. Spalling and slinging pattern of shallow slope and dynamics explanation in the 2008 Wenchuan earthquake. In Proceedings of the 10th Conference on Rock Mechanics and Engineering, China, 2009: 258-262.

Tang C, Van Western CJ, Tanyas H et al (2016) Analysing post-earthquake landslide activity using multi-temporal landslide inventories near the epicentral area of the 2008 Wenchuan earthquake. Natural Hazards and Earth System Sciences 16:2641–2655

The Earthquake Disaster Prevention Department of China Earthquake Administration (1995) Catalogue of Chinese historical strong earthquakes (in Chinese). Seismological Press, Beijing, pp 1–514

The Earthquake Disaster Prevention Department of China Earthquake Administration (1999) Catalogue of Chinese present earthquakes (in Chinese). China Science and Technology Press, Beijing, pp 1–637

Tian Y, Xu C, Ma S et al (2019) Inventory and space distribution of landslides triggered by the 8th August 2017 $M_w$ 6.5 Jiuzhaigou earthquake, China. Journal of Earth Science 30(1):206–217

Tian Y, Owen LA, Xu C (2020) etc. Landslide development within 3 years after the 2015 $M_w$ 7.8 Gorkha earthquake, Nepal. Landslides 17:1251–1267

UNESCO. World heritage nomination-advisory body evaluation (IUCN). 637: Jiuzhaigou Valley scenic and historic interest area (China), 1992. Website: http://whc.unesco.org/document/153932. Accessed 14 October 2017.

Vanani AGG, Shoaei G, Zare M Statistical analyses of landslide size and spatial distribution triggered by 1990 Rudbar-Manjil ($M_w$ 7.3) earthquake, northern Iran: revised inventory, and controlling factors. Bulletin of Engineering Geology and the Environment, 2021: 80(4):3381–3403

Wang YS, Huang RQ, Luo YH (2011) etc. The genetic mechanism of Wenchuan earthquake. Journal of Mountain Sciences 8:336–344

Wang J, Jin W, Cui Y et al (2018) Earthquake-triggered landslides affecting a UNESCO Natural Site: the 2017 Jiuzhaigou Earthquake in the World National Park, China. Journal of Mountain Sciences 15(7): 1412–1428

Woo MK, Luk SH (1990) Vegetation effects on soil and water losses on weathered granitic hillslopes. South China. Physical Geography 11(1):1–16

Wu C, Cui P, Li Y et al (2018) Seismogenic fault and topography control on the spatial patterns of landslides triggered by the 2017 Jiuzhaigou earthquake. Journal of Mountain Sciences 14(4):793–807

Xu C (2015) Preparation of earthquake-triggered landslide inventory maps using remote sensing and GIS technologies: principles and case studies. Geoscience Frontiers 6:825–836

Xu C (2018) Landslide seismology geology: a sub-discipline of environmental earth sciences. Journal of Engineering Geology 26(1):207–222

Xu Q, Li W (2010) Study on the direction effects of landslides triggered by Wenchuan earthquake. Journal of Sichuan University (Engineering Science Edition) 42(z1):7–14

Xu Q, Zhang S, Li W (2011) Spatial distribution of large-scale landslides induced by the 5.12 Wenchuan earthquake. Journal of Mountain Science 8(2):246–260

Xu C, Xu X, Yao X et al (2014) Three nearly complete inventories of landslides triggered by the May 12, 2008 Wenchuan $M_w$ 7.9 earthquake of China and their spatial distribution statistical analysis. Landslides 11:441–461

Xu C, Xu X, Tian Y et al (2016a) Two comparable earthquakes produced greatly different coseismic landslides: the 2015 Gorkha, Nepal and 2008 Wenchuan, China events. Journal of Earth Science 27(6): 1008–1015

Xu C, Xu X, Shen L (2016b) etc. Optimized volume models of earthquake-triggered landslides. Scientific Reports 6(1):559–576

Xu X, Chen G, Wang Q (2017) etc. Discussion on seismogenic structure of Jiuzhaigou earthquake and its implication for current strain state in the southeastern Qinghai-Tibet Plateau. Chinese Journal of Geophysics 60(10):4018–4026

Xu C, Wang S, Xu X et al (2018) A panorama of landslides triggered by the 8 August 2017 Jiuzhaigou, Sichuan $M_s$ 7.0 earthquake. Seismology and Geology 40(1):232–260

Yang W, Qi W, Zhou J (2018a) Decreased post-seismic landslides linked to vegetation recovery after the 2008 Wenchuan earthquake. Ecological Indicators 89:438–444

Yang Z, Xiong F, Yu M (2018b) etc. Research on the earthquake disaster area of Jiuzhaigou and the reflection of reconstruction mode. China Civil Engineering Journal 51(S2):41–47

Yi G, Long F, Liang M et al (2017) Focal mechanism solutions and seismogenic structure of the 8 August 2017 M 7.0 Jiuzhaigou earthquake and its aftershocks, northern Sichuan. Chinese Journal of Geophysics 60(10):4083–4097

Yi Y, Zhang Z, Zhang W et al (2019) GIS-based earthquake-triggered-landslide susceptibility mapping with an integrated weighted index model in Jiuzhaigou region of Sichuan Province, China. Natural Hazards and Earth System Sciences 19(9):1973–1988

Yue X, Wu S, Yin Y et al (2018) Risk identification of seismic landslides by joint Newmark and RockFall analyst models: a case study of roads affected by the Jiuzhaigou Earthquake. International Journal of Disaster Risk Science 9:392–406

Yunus AP, Fan X, Tang X, Jie D, Xu Q, Huang R (2020) Decadal vegetation succession from MODIS reveals the spatio-temporal evolution of post-seismic landsliding after the 2008 Wenchuan earthquake. Remote Sensing of Environment 237:111541

Zhang S, Zhang L (2017) Impact of the 2008 Wenchuan earthquake in China on subsequent long-term debris flow activities in the epicentral area. Geomorphology 276:86–103

Zhang LM, Zhang S, Huang RQ (2014) Multi-hazard scenarios and consequences in Beichuan, China: the first five years after the 2008 Wenchuan earthquake. Engineering Geology 180:4–20

Zhang S., Zhang L., Lacasse S., etc. Evolution of mass movements near epicenter of Wenchuan Earthquake, the first eight years. Scientific Reports, 2016, 6: 36154.

Zhao B, Xu X (2008) An analysis on $M_s$ 8.0 Wenchuan earthquake fault and seismic disaster. Seismology and Geology 30(4):839–853

Zhao B, Wang Y, Luo Y et al (2018) Landslides and dam damage resulting from the Jiuzhaigou earthquake (8 August 2017), Sichuan, China. Royal Society Open Science 5:171418